10-1-1999

# Measurement of $B^0$-$\bar{B}^0$ flavor oscillations using jet-charge and lepton flavor tagging in $p\bar{p}$ collisions at √s =1.8 TeV

F. Abe
*National Laboratory for High Energy Physics (KEK), Tsukuba, Ibaraki 305, Japan*

Kenneth A. Bloom
*University of Nebraska-Lincoln*, kenbloom@unl.edu

Collider Detector at Fermilab Collaboration

# Measurement of $B^0$-$\bar{B}^0$ flavor oscillations using jet-charge and lepton flavor tagging in $p\bar{p}$ collisions at $\sqrt{s}=1.8$ TeV

F. Abe,[17] H. Akimoto,[39] A. Akopian,[31] M. G. Albrow,[7] S. R. Amendolia,[27] D. Amidei,[20] J. Antos,[33] S. Aota,[37] G. Apollinari,[31] T. Arisawa,[39] T. Asakawa,[37] W. Ashmanskas,[5] M. Atac,[7] P. Azzi-Bacchetta,[25] N. Bacchetta,[25] S. Bagdasarov,[31] M. W. Bailey,[22] P. de Barbaro,[30] A. Barbaro-Galtieri,[18] V. E. Barnes,[29] B. A. Barnett,[15] M. Barone,[9] G. Bauer,[19] T. Baumann,[11] F. Bedeschi,[27] S. Behrends,[3] S. Belforte,[27] G. Bellettini,[27] J. Bellinger,[40] D. Benjamin,[6] J. Bensinger,[3] A. Beretvas,[7] J. P. Berge,[7] J. Berryhill,[5] S. Bertolucci,[9] S. Bettelli,[27] B. Bevensee,[26] A. Bhatti,[31] K. Biery,[7] C. Bigongiari,[27] M. Binkley,[7] D. Bisello,[25] R. E. Blair,[1] C. Blocker,[3] K. Bloom,[20] S. Blusk,[30] A. Bodek,[30] W. Bokhari,[26] G. Bolla,[29] Y. Bonushkin,[4] D. Bortoletto,[29] J. Boudreau,[28] A. Brandl,[22] L. Breccia,[2] C. Bromberg,[21] N. Bruner,[22] R. Brunetti,[2] E. Buckley-Geer,[7] H. S. Budd,[30] K. Burkett,[11] G. Busetto,[25] A. Byon-Wagner,[7] K. L. Byrum,[1] M. Campbell,[20] A. Caner,[27] W. Carithers,[18] D. Carlsmith,[40] J. Cassada,[30] A. Castro,[25] D. Cauz,[36] A. Cerri,[27] P. S. Chang,[33] P. T. Chang,[33] H. Y. Chao,[33] J. Chapman,[20] M.-T. Cheng,[33] M. Chertok,[34] G. Chiarelli,[27] C. N. Chiou,[33] F. Chlebana,[7] L. Christofek,[13] M. L. Chu,[33] S. Cihangir,[7] A. G. Clark,[10] M. Cobal,[27] E. Cocca,[27] M. Contreras,[5] J. Conway,[32] J. Cooper,[7] M. Cordelli,[9] D. Costanzo,[27] C. Couyoumtzelis,[10] D. Cronin-Hennessy,[6] R. Cropp,[14] R. Culbertson,[5] D. Dagenhart,[38] T. Daniels,[19] F. DeJongh,[7] S. Dell'Agnello,[9] M. Dell'Orso,[27] R. Demina,[7] L. Demortier,[31] M. Deninno,[2] P. F. Derwent,[7] T. Devlin,[32] J. R. Dittmann,[6] S. Donati,[27] J. Done,[34] T. Dorigo,[25] N. Eddy,[13] K. Einsweiler,[18] J. E. Elias,[7] R. Ely,[18] E. Engels, Jr.,[28] W. Erdmann,[7] D. Errede,[13] S. Errede,[13] Q. Fan,[30] R. G. Feild,[41] Z. Feng,[15] C. Ferretti,[27] I. Fiori,[2] B. Flaugher,[7] G. W. Foster,[7] M. Franklin,[11] J. Freeman,[7] J. Friedman,[19] Y. Fukui,[17] S. Gadomski,[14] S. Galeotti,[27] M. Gallinaro,[26] O. Ganel,[35] M. Garcia-Sciveres,[18] A. F. Garfinkel,[29] C. Gay,[41] S. Geer,[7] D. W. Gerdes,[20] P. Giannetti,[27] N. Giokaris,[31] P. Giromini,[9] G. Giusti,[27] M. Gold,[22] A. Gordon,[11] A. T. Goshaw,[6] Y. Gotra,[28] K. Goulianos,[31] H. Grassmann,[36] C. Green,[29] L. Groer,[32] C. Grosso-Pilcher,[5] G. Guillian,[20] J. Guimaraes da Costa,[15] R. S. Guo,[33] C. Haber,[18] E. Hafen,[19] S. R. Hahn,[7] R. Hamilton,[11] T. Handa,[12] R. Handler,[40] W. Hao,[35] F. Happacher,[9] K. Hara,[37] A. D. Hardman,[29] R. M. Harris,[7] F. Hartmann,[16] J. Hauser,[4] E. Hayashi,[37] J. Heinrich,[26] A. Heiss,[16] B. Hinrichsen,[14] K. D. Hoffman,[29] C. Holck,[26] R. Hollebeek,[26] L. Holloway,[13] Z. Huang,[20] B. T. Huffman,[28] R. Hughes,[23] J. Huston,[21] J. Huth,[11] H. Ikeda,[37] M. Incagli,[27] J. Incandela,[7] G. Introzzi,[27] J. Iwai,[39] Y. Iwata,[12] E. James,[20] H. Jensen,[7] U. Joshi,[7] E. Kajfasz,[25] H. Kambara,[10] T. Kamon,[34] T. Kaneko,[37] K. Karr,[38] H. Kasha,[41] Y. Kato,[24] T. A. Keaffaber,[29] K. Kelley,[19] M. Kelly,[20] R. D. Kennedy,[7] R. Kephart,[7] D. Kestenbaum,[11] D. Khazins,[6] T. Kikuchi,[37] M. Kirk,[3] B. J. Kim,[27] H. S. Kim,[14] S. H. Kim,[37] Y. K. Kim,[18] L. Kirsch,[3] S. Klimenko,[8] D. Knoblauch,[16] P. Koehn,[23] A. Köngeter,[16] K. Kondo,[37] J. Konigsberg,[8] K. Kordas,[14] A. Korytov,[8] E. Kovacs,[1] W. Kowald,[6] J. Kroll,[26] M. Kruse,[30] S. E. Kuhlmann,[1] E. Kuns,[32] K. Kurino,[12] T. Kuwabara,[37] A. T. Laasanen,[29] S. Lami,[27] S. Lammel,[7] J. I. Lamoureux,[3] M. Lancaster,[18] M. Lanzoni,[27] G. Latino,[27] T. LeCompte,[1] A. M. Lee IV,[6] S. Leone,[27] J. D. Lewis,[7] M. Lindgren,[4] T. M. Liss,[13] J. B. Liu,[30] Y. C. Liu,[33] N. Lockyer,[26] O. Long,[26] M. Loreti,[25] D. Lucchesi,[27] P. Lukens,[7] S. Lusin,[40] J. Lys,[18] K. Maeshima,[7] P. Maksimovic,[11] M. Mangano,[27] M. Mariotti,[25] J. P. Marriner,[7] G. Martignon,[25] A. Martin,[41] J. A. J. Matthews,[22] P. Mazzanti,[2] K. McFarland,[30] P. McIntyre,[34] P. Melese,[31] M. Menguzzato,[25] A. Menzione,[27] E. Meschi,[27] S. Metzler,[26] C. Miao,[20] T. Miao,[7] G. Michail,[11] R. Miller,[21] H. Minato,[37] S. Miscetti,[9] M. Mishina,[17] S. Miyashita,[37] N. Moggi,[27] E. Moore,[22] Y. Morita,[17] A. Mukherjee,[7] T. Muller,[16] A. Munar,[27] P. Murat,[27] S. Murgia,[21] M. Musy,[36] H. Nakada,[37] T. Nakaya,[5] I. Nakano,[12] C. Nelson,[7] D. Neuberger,[16] C. Newman-Holmes,[7] C.-Y. P. Ngan,[19] H. Niu,[3] L. Nodulman,[1] A. Nomerotski,[8] S. H. Oh,[6] T. Ohmoto,[12] T. Ohsugi,[12] R. Oishi,[37] M. Okabe,[37] T. Okusawa,[24] J. Olsen,[40] C. Pagliarone,[27] R. Paoletti,[27] V. Papadimitriou,[35] S. P. Pappas,[41] N. Parashar,[27] A. Parri,[9] D. Partos,[3] J. Patrick,[7] G. Pauletta,[36] M. Paulini,[18] A. Perazzo,[27] L. Pescara,[25] M. D. Peters,[18] T. J. Phillips,[6] G. Piacentino,[27] M. Pillai,[30] K. T. Pitts,[7] R. Plunkett,[7] A. Pompos,[29] L. Pondrom,[40] J. Proudfoot,[1] F. Ptohos,[11] G. Punzi,[27] K. Ragan,[14] D. Reher,[18] A. Ribon,[25] F. Rimondi,[2] L. Ristori,[27] W. J. Robertson,[6] A. Robinson,[14] T. Rodrigo,[27] S. Rolli,[38] L. Rosenson,[19] R. Roser,[7] T. Saab,[14] W. K. Sakumoto,[30] D. Saltzberg,[4] A. Sansoni,[9] L. Santi,[36] H. Sato,[37] P. Schlabach,[7] E. E. Schmidt,[7] M. P. Schmidt,[41] A. Scott,[4] A. Scribano,[27] S. Segler,[7] S. Seidel,[22] Y. Seiya,[37] F. Semeria,[2] T. Shah,[19] M. D. Shapiro,[18] N. M. Shaw,[29] P. F. Shepard,[28] T. Shibayama,[37] M. Shimojima,[37] M. Shochet,[5] J. Siegrist,[18] A. Sill,[35] P. Sinervo,[14] P. Singh,[13] K. Sliwa,[38] C. Smith,[15] F. D. Snider,[7] J. Spalding,[7] T. Speer,[10] P. Sphicas,[19] F. Spinella,[27] M. Spiropulu,[11] L. Spiegel,[7] L. Stanco,[25] J. Steele,[40] A. Stefanini,[27] R. Ströhmer,[7,*] J. Strologas,[13] F. Strumia,[10] D. Stuart,[7] K. Sumorok,[19] J. Suzuki,[37] T. Suzuki,[37] T. Takahashi,[24] T. Takano,[24] R. Takashima,[12] K. Takikawa,[37] M. Tanaka,[37] B. Tannenbaum,[4] F. Tartarelli,[27] W. Taylor,[14] M. Tecchio,[20] P. K. Teng,[33] Y. Teramoto,[24] K. Terashi,[37] S. Tether,[19] D. Theriot,[7] T. L. Thomas,[22] R. Thurman-Keup,[1] M. Timko,[38] P. Tipton,[30] A. Titov,[31] S. Tkaczyk,[7] D. Toback,[5] K. Tollefson,[30] A. Tollestrup,[7] H. Toyoda,[24] W. Trischuk,[14] J. F. de Troconiz,[11] S. Truitt,[20] J. Tseng,[19] N. Turini,[27] T. Uchida,[37] F. Ukegawa,[26] J. Valls,[32] S. C. van den Brink,[15] S. Vejcik III,[7] G. Velev,[27] R. Vidal,[7] R. Vilar,[7,*] I. Vologouev,[18] D. Vucinic,[19] R. G. Wagner,[1] R. L. Wagner,[7] J. Wahl,[5] N. B. Wallace,[27] A. M. Walsh,[32] C. Wang,[6] C. H. Wang,[33] M. J. Wang,[33] A. Warburton,[14] T. Watanabe,[37] T. Watts,[32] R. Webb,[34] C. Wei,[6] H. Wenzel,[16] W. C. Wester III,[7] A. B. Wicklund,[1] E. Wicklund,[7] R. Wilkinson,[26] H. H. Williams,[26] P. Wilson,[7] B. L. Winer,[23] D. Winn,[20] D. Wolinski,[20] J. Wolinski,[21] S. Worm,[22] X. Wu,[10] J. Wyss,[27] A. Yagil,[7] W. Yao,[18] K. Yasuoka,[37] G. P. Yeh,[7] P. Yeh,[33] J. Yoh,[7] C. Yosef,[21] T. Yoshida,[24] I. Yu,[7] A. Zanetti,[36] F. Zetti,[27] and S. Zucchelli[2]

 

(CDF Collaboration)
[1]*Argonne National Laboratory, Argonne, Illinois 60439*
[2]*Istituto Nazionale di Fisica Nucleare, University of Bologna, I-40127 Bologna, Italy*
[3]*Brandeis University, Waltham, Massachusetts 02254*
[4]*University of California at Los Angeles, Los Angeles, California 90024*
[5]*University of Chicago, Chicago, Illinois 60637*
[6]*Duke University, Durham, North Carolina 27708*
[7]*Fermi National Accelerator Laboratory, Batavia, Illinois 60510*
[8]*University of Florida, Gainesville, Florida 32611*
[9]*Laboratori Nazionali di Frascati, Istituto Nazionale di Fisica Nucleare, I-00044 Frascati, Italy*
[10]*University of Geneva, CH-1211 Geneva 4, Switzerland*
[11]*Harvard University, Cambridge, Massachusetts 02138*
[12]*Hiroshima University, Higashi-Hiroshima 724, Japan*
[13]*University of Illinois, Urbana, Illinois 61801*
[14]*Institute of Particle Physics, McGill University, Montreal, Quebec H3A 2T8*
*and University of Toronto, Toronto, Ontario, Canada, M5S 1A7*
[15]*The Johns Hopkins University, Baltimore, Maryland 21218*
[16]*Institut für Experimentelle Kernphysik, Universität Karlsruhe, D-76128 Karlsruhe, Germany*
[17]*National Laboratory for High Energy Physics (KEK), Tsukuba, Ibaraki 305, Japan*
[18]*Ernest Orlando Lawrence Berkeley National Laboratory, Berkeley, California 94720*
[19]*Massachusetts Institute of Technology, Cambridge, Massachusetts 02139*
[20]*University of Michigan, Ann Arbor, Michigan 48109*
[21]*Michigan State University, East Lansing, Michigan 48824*
[22]*University of New Mexico, Albuquerque, New Mexico 87131*
[23]*The Ohio State University, Columbus, Ohio 43210*
[24]*Osaka City University, Osaka 588, Japan*
[25]*Universita di Padova, Istituto Nazionale di Fisica Nucleare, Sezione di Padova, I-35131 Padova, Italy*
[26]*University of Pennsylvania, Philadelphia, Pennsylvania 19104*
[27]*Istituto Nazionale di Fisica Nucleare, University and Scuola Normale Superiore of Pisa, I-56100 Pisa, Italy*
[28]*University of Pittsburgh, Pittsburgh, Pennsylvania 15260*
[29]*Purdue University, West Lafayette, Indiana 47907*
[30]*University of Rochester, Rochester, New York 14627*
[31]*Rockefeller University, New York, New York 10021*
[32]*Rutgers University, Piscataway, New Jersey 08855*
[33]*Academia Sinica, Taipei, Taiwan 11530, Republic of China*
[34]*Texas A & M University, College Station, Texas 77843*
[35]*Texas Tech University, Lubbock, Texas 79409*
[36]*Istituto Nazionale di Fisica Nucleare, University of Trieste/Udine, Italy*
[37]*University of Tsukuba, Tsukuba, Ibaraki 305, Japan*
[38]*Tufts University, Medford, Massachusetts 02155*
[39]*Waseda University, Tokyo 169, Japan*
[40]*University of Wisconsin, Madison, Wisconsin 53706*
[41]*Yale University, New Haven, Connecticut 06520*
(Received 16 March 1999; published 10 September 1999)

We present a measurement of the mass difference $\Delta m_d$ for the $B^0$ meson and the statistical power of the $b$ flavor tagging methods used. The measurement uses 90 $\mathrm{pb}^{-1}$ of data from $p\bar{p}$ collisions at $\sqrt{s}=1.8$ TeV collected with the CDF detector. An inclusive lepton trigger is used to collect a large sample of $B$ hadron semileptonic decays. The mass difference $\Delta m_d$ is determined from the proper time dependence of the fraction of $B$ hadrons that undergo flavor oscillations. The flavor at decay is inferred from the charge of the lepton from semileptonic $B$ decay. The initial flavor is inferred by determining the flavor of the other $B$ hadron produced in the collision, either from its semileptonic decay (soft-lepton tag) or from its jet charge. The measurement yields $\Delta m_d=(0.500\pm0.052\pm0.043)\hbar\ \mathrm{ps}^{-1}$, where the first uncertainty is statistical and the second uncertainty is systematic. The statistical powers ($\epsilon D^2$) of the soft-lepton and jet-charge flavor taggers are $(0.91\pm0.10\pm0.11)\%$ and $(0.78\pm0.12\pm0.08)\%$, respectively. [S0556-2821(99)05417-X]

PACS number(s): 12.15.Ff, 13.20.He, 14.40.Nd

*Visitor.

## I. INTRODUCTION

In the standard model of electroweak interactions [1], the quark mass eigenstates are related to the weak eigenstates via the unitary $3\times3$ Cabibbo-Kobayashi-Maskawa (CKM) matrix $V_{\rm CKM}$ [2]. The nine elements in this matrix, $V_{ij}$, where $i=u,c,t$ and $j=d,s,b$, are completely determined from three angles and a phase. A nonzero phase gives $CP$ violation in the weak interaction. Measurements of decays of hadrons containing $b$ quarks ($B$ hadrons) are of great interest because they determine the magnitudes of five of the nine elements of $V_{\rm CKM}$ as well as the phase.

### A. Unitarity triangle

The unitarity of $V_{\rm CKM}$ leads to nine unitarity relationships, one of which is of particular interest:

$$V_{ud}V_{ub}^*+V_{cd}V_{cb}^*+V_{td}V_{tb}^*=0. \tag{1.1}$$

This sum of three complex numbers forms a triangle in the complex plane. This triangle is commonly referred to as *the* unitarity triangle. Measurements of the weak decays of $B$ hadrons and the already known CKM matrix elements determine the magnitudes of the three sides of the unitarity triangle, and $CP$ asymmetries in $B$ meson decays determine the three angles. The primary goal of $B$ physics in the next decade is to measure precisely both the sides and angles of this triangle and test consistency within the standard model.

We can use several approximations to express Eq. (1.1) in a more convenient form. The elements $V_{ud}\simeq1$ and $V_{cd}\simeq-\lambda=-\sin\theta_{\rm C}$, where $\theta_{\rm C}$ is the Cabibbo angle, are well measured. Although the elements $V_{tb}$ and $V_{ts}$ are not well measured, the theoretical expectations are that $V_{tb}\simeq1$ and $V_{ts}\simeq-V_{cb}^*$. With these assumptions, Eq. (1.1) becomes

$$\frac{V_{ub}^*}{\lambda V_{cb}^*}-1-\frac{V_{td}}{\lambda V_{ts}}=0. \tag{1.2}$$

Measurement of $\Delta m_d$, the subject of this paper, directly impacts the determination of $V_{td}/V_{ts}$.

### B. Determining $V_{td}$ and $V_{ts}$ from neutral $B$ meson flavor oscillations

Second-order weak processes transform a neutral $B$ meson into its antiparticle: $B^0\to\overline{B^0}$, giving a probability for a $B^0$ to decay as a $\overline{B^0}$ that oscillates with time. The frequency of these oscillations is the mass difference $\Delta m_d$ between the $B$ mass eigenstates, which are linear combinations of the flavor eigenstates $B^0$ and $\overline{B^0}$. The mass difference is proportional to $|V_{tb}^*V_{td}|^2$, so in principle, a measurement of $\Delta m_d$ determines this product of CKM matrix elements. In practice, however, large theoretical uncertainties limit the precision of $V_{td}$. The same problem exists in determining $V_{ts}$ from $\Delta m_s$, the frequency of $B_s^0\to\overline{B_s^0}$ oscillations. These theoretical uncertainties are reduced in determining the ratio $|V_{td}/V_{ts}|^2$ from $\Delta m_d/\Delta m_s$. Unfortunately, at this time, attempts to measure $\Delta m_s$ have only led to lower limits. The determination of $\Delta m_s$ is a key future measurement of $B$ hadrons, since $|V_{td}/V_{ts}|^2$ determines the magnitude of one of the sides of the unitarity triangle, as expressed in Eq. (1.2).

Measurements of $\Delta m_d$ and $\Delta m_s$ require determining the initial flavor of the $B$ meson, that is, whether the $B$ meson contained a $b$ quark or a $\overline{b}$ antiquark. Flavor determination is also crucial in the measurement of $CP$ violation in the decays of neutral $B$ mesons to $CP$ eigenstates.

This paper describes a measurement of $\Delta m_d$ using data collected by the Collider Detector at Fermilab (CDF) experiment from $p\overline{p}$ collisions with a center-of-mass energy of 1.8 TeV produced by the Fermilab Tevatron. In addition, the measurement of $\Delta m_d$ is used to demonstrate the performance of two methods (described below) of identifying the flavor of $B$ hadrons in the environment of $p\overline{p}$ collisions. These methods of flavor identification will be important in the measurement of $CP$ violation in the decays of neutral $B$ mesons and in the study of $\Delta m_s$ [3].

### C. Previous measurements of $\Delta m_d$ from CDF

The CDF Collaboration has exploited the large $b$ quark production cross section at the Fermilab Tevatron to make several precision measurements of the properties of $B$ hadrons, including lifetimes and masses [4]. Although the $b$ quark production cross section at the Tevatron is large, the $p\overline{p}$ inelastic cross section is three orders of magnitude larger, so specialized triggers are required to collect large samples of $B$ hadrons. To date, the triggers that have been utilized are based on leptons (electrons and muons) or dileptons. Some analyses use the semileptonic decays of $B$ hadrons, $B\to l\nu X$, some use the semileptonic decays of charmed particles from $B$ hadron decay (e.g. $B\to DX$, followed by $D\to l\nu Y$), and some use leptonic $J/\psi$ decays ($B\to J/\psi X$, followed by $J/\psi\to\mu^+\mu^-$).

Previous measurements of $\Delta m_d$ from CDF were based on data samples collected with a dimuon trigger [5] and single-lepton triggers ($l=e,\mu$) [6]. The single-lepton triggers were used to partially reconstruct approximately 6000 $B^0$ mesons via their semileptonic decays $B^0\to l^+\nu D^{(*)-}X$ (in this paper, reference to a particular decay sequence implies the charge-conjugate sequence as well). The analysis reported in this paper uses the same data sample collected with this trigger, but increases the number of $B$ mesons by over an order of magnitude by inclusively reconstructing $B$ hadrons that decay semileptonically. The inclusive reconstruction is made possible by the relatively long lifetime of $B$ hadrons: the decay point of the $B$ hadron is typically separated from the production point (the primary vertex) by a couple of millimeters. The inclusive reconstruction is based on identifying this decay point by associating the trigger lepton with other charged decay products to reconstruct a secondary vertex.

### D. Method of measuring $\Delta m_d$

The oscillation frequency $\Delta m_d$ can be found from either a time independent measurement (that is, from the total num-

ber of $B^0$'s that decay as $\overline{B^0}$'s) or from a time dependent measurement (that is, from the rates that a state that is pure $B^0$ at $t=0$ decays as either a $\overline{B^0}$ or $B^0$ as a function of proper decay time $t$). The latter technique has better sensitivity and allows a simultaneous study of the tagging methods since the amplitude of the oscillation depends on the effectiveness of the tagging method.

The expected rate is

$$\mathcal{P}(B^0 \to B^0) = \frac{1}{2\tau_B} e^{-t/\tau_B}[1+\cos(\Delta m_d t)], \qquad (1.3)$$

$$\mathcal{P}(B^0 \to \overline{B^0}) = \frac{1}{2\tau_B} e^{-t/\tau_B}[1-\cos(\Delta m_d t)], \qquad (1.4)$$

where $\tau_B$ is the mean lifetime of the two mass eigenstates of the $B^0$ (the difference in lifetime of these two eigenstates is very small [7] and has been neglected), and $t$ is the proper decay time of the $B^0$ in its rest frame. To measure this rate, we need to make three measurements: (1) the proper decay time, (2) the $B$ flavor at decay, and (3) the produced $B$ flavor. We determine the proper time by measuring the distance from the production point to the decay point in the laboratory frame combined with an estimate of the $B^0$ momentum. The flavor at decay is determined from the charge of the lepton, assuming it comes from semileptonic $B$ decay. In our measurement [6] of $\Delta m_d$ using $B^0 \to l^+ \nu D^{(*)-} X$ decays, the flavor at production was identified using a same-side tagging technique based on the electric charge of particles produced in association with the $B^0$. This flavor tag has also been applied [8] to a sample of $B^0/\overline{B^0} \to J/\psi K_S^0$ decays to measure the $CP$ asymmetry. To identify the flavor at production in this analysis, we rely on the fact that the dominant production mechanisms of $b$ quarks in $p\overline{p}$ collisions produce $b\overline{b}$ pairs. The flavors of the $B$ hadrons are assumed to be opposite at the time of production. In this paper, we identify the flavor of the other $B$ hadron using two techniques: the soft-lepton flavor tag (SLT) and the jet-charge flavor tag (JCT).

Several precise measurements of $\Delta m_d$ have been published [9] by experiments operating on the $\Upsilon(4S)$ and $Z^0$ resonances. The measurement of $\Delta m_d$ presented here is competitive in precision and in addition quantifies the performance of the flavor tags, which are crucial for future measurements of $CP$ violation in the decays of $B$ mesons and the measurement of $\Delta m_s$ at a hadron collider. The jet-charge flavor tag is a powerful technique in studies of neutral $B$ meson flavor oscillations by experiments operating on the $Z^0$ resonance [10]. This analysis is the first application of the jet-charge flavor tag in the environment of a hadron collider.

## II. CDF DETECTOR

The data sample used in this analysis was collected from 90 $\text{pb}^{-1}$ of $p\overline{p}$ collisions recorded with the CDF detector at the Fermilab Tevatron. The CDF detector is described in detail elsewhere [11,12]. We summarize here the features of the detector that are important for this analysis. The CDF coordinate system has the $z$ axis pointing along the proton momentum, with the $x$ axis located in the horizontal plane of the Tevatron storage ring, pointing radially outward, so that the $y$ axis points up. The coordinates $r$, $\phi$, and $\theta$ are the standard cylindrical coordinates.

The CDF spectrometer consists of three separate detectors for tracking charged particles: the silicon vertex detector (SVX), the vertex detector (VTX), and the central tracking chamber (CTC), which are immersed in a magnetic field of 1.4 T pointed along the $+z$ axis. The SVX [13] consists of four concentric cylinders of single-sided silicon strip detectors positioned at radii between 3 cm and 8 cm from the beam line. The strips are oriented parallel to the beam axis and have a pitch of 60 $\mu$m in the inner three layers and 55 $\mu$m on the outermost layer. The SVX is surrounded by the VTX, which is used to determine the $z$ coordinate of the $p\overline{p}$ interaction (the primary vertex). Surrounding the SVX and VTX is the CTC. The CTC is a drift chamber that is 3.2 m long with 84 layers of sense wires located between a radius of 31 cm and 133 cm. The sense wires are organized into five axial superlayers and four stereo superlayers with a stereo angle of 3°. The momentum resolution of the spectrometer is $\delta p_T/p_T = [(0.0009\ (\text{GeV}/c)^{-1} p_T)^2 + (0.0066)^2]^{1/2}$, where $p_T$ is the component of momentum transverse to the $z$ axis ($p_T = p \sin\theta$). Charged particle trajectories reconstructed in the CTC that are matched to strip clusters in the SVX have an impact parameter resolution of $\delta d_0 = [13 + (40\ \text{GeV}/c)/p_T]$ $\mu$m, where the impact parameter $d_0$ is the distance of closest approach of the trajectory to the beam axis in the plane perpendicular to the beam axis. The outer 54 layers of the CTC are instrumented to record the ionization ($dE/dx$) of charged tracks.

Surrounding the CTC are the central electromagnetic calorimeter (CEM) and the central hadronic calorimeter (CHA). The CEM has strip chambers (CES) positioned at shower maximum and a preshower detector (CPR) located at a depth of one radiation length. Beyond the central calorimeters lie two sets of muon detectors. To reach these two detectors, particles produced at the primary vertex with a polar angle of 90° must traverse material totaling 5.4 and 8.4 pion interaction lengths, respectively. The trigger system consists of three levels: the first two levels are implemented in hardware. The third level consists of software reconstruction algorithms that reconstruct the data, including three-dimensional track reconstruction in the CTC using a fast algorithm that is efficient only for $p_T > 1.4$ GeV/$c$.

## III. DATA SAMPLE SELECTION

The sample selection begins with data from the inclusive $e$ and $\mu$ triggers. At level 2, both of these triggers require a track with $p_T > 7.5$ GeV/$c$ found by the central fast tracker (CFT) [14], a hardware track processor that uses fast timing information from the CTC as input. The resolution of the CFT is $\delta p_T/p_T = 0.035\ (\text{GeV}/c)^{-1} p_T$. In the case of the electron trigger, the CFT track must be matched to a cluster in the electromagnetic calorimeter, with transverse energy $E_T > 8.0$ GeV, where $E_T = E \sin\theta$, and $E$ is the energy of the calorimeter cluster. In the case of the muon trigger, the CFT track must be matched to a reconstructed track segment in

both sets of muon detectors. In the third level of the trigger, more stringent electron and muon selection criteria, which are similar to the selection criteria described in Sec. III A, are applied. The inclusive electron data set contains approximately $5.6\times10^6$ events and the inclusive muon data set contains approximately $2.0\times10^6$ events. These data are dominated by leptons from the decay of heavy flavors ($b\rightarrow l$ and $c\rightarrow l$) and hadrons that mimic the lepton signal.

### A. Electron and muon identification

Electron candidates are identified using information from both the calorimeters and the tracking detectors. The electron calorimeter cluster in the CEM must have $E_T>6$ GeV. The longitudinal shower profile of this cluster is required to be consistent with an electron shower with a leakage energy from the CEM into the CHA of less than 4%. The lateral shower profile of the CEM cluster has to be consistent with the profile determined from test beam electrons. A track with $p_t>6$ GeV/$c$ must match the electron calorimeter cluster. This match is based on a comparison of the track position with the calorimeter cluster position determined in the CES: the difference between the extrapolated position of the track and the position of the cluster centroid must satisfy $r|\Delta\varphi|<1.5$ cm and $|\Delta z\sin\theta|<3$ cm.

To identify muons, we require a match between the extrapolated CTC track and the track segment in the muon chamber in both the $r$-$\varphi$ and $r$-$z$ views. The uncertainty in this match is taken into account and is dominated by multiple scattering in the detector material. The transverse muon momentum must satisfy $p_T>6$ GeV/$c$.

Finally, to ensure optimal resolution of the $B$ hadron decay point, the electron and muon candidate tracks have to be reconstructed in the SVX detector.

### B. Jet reconstruction

Further analysis of the data sample is based on the charged-particle jets in the event. Charged particles (instead of the more commonly used calorimeter clusters) are used to form jets in order to keep the electron and muon samples as similar as possible. These jets are found using a cone clustering algorithm. Tracks with $p_T>1.0$ GeV/$c$ are used as jet seeds. If two seeds are within $\Delta R<0.7$ [15], the momenta of the seeds are added together to form a new seed. After all possible seed merging, lower momentum tracks ($0.4<p_T<1.0$ GeV/$c$) that are within $\Delta R<0.7$ of a seed are added in to form the final jets. The trigger lepton is always associated to a jet, and below we refer to this jet as the trigger-lepton jet. A jet can consist of a single track with $p_T>1$ GeV/$c$.

### C. Secondary vertex reconstruction

In order to reconstruct the time of decay in the $B$ rest frame (the proper time), we must measure the point of decay with respect to the primary interaction in the laboratory and estimate the momentum of the $B$. Since the SVX provides only coordinates in the plane transverse to the beam axis, the measurement of the separation between the point of decay and the primary vertex is done only in the $x$-$y$ plane. We refer to this separation as the decay length $L_{xy}$. Only the component of the $B$ momentum transverse to the beam axis ($p_T^B$) is needed to calculate the proper time at decay, since the decay length is measured in the $x$-$y$ plane.

The positions of the $p\overline{p}$ interactions or ''primary vertices'' are distributed along the beam direction according to a Gaussian with a width of $\sim30$ cm. In the plane transverse to the beam axis, these interactions follow a distribution that is a Gaussian with a width of $\sim25$ $\mu$m in both the $x$ and $y$ dimensions. To reconstruct the primary event vertex, we first identify its $z$ position using the tracks reconstructed in the VTX detector. When projected back to the beam axis, these tracks determine the longitudinal location of the primary interaction with a precision of about 0.2 cm along the beam direction. If there is more than one reconstructed primary vertex in an event, the trigger lepton is associated with the primary vertex closest in $z$ to the intercept of the trigger lepton with the beam line.

The transverse position of the primary vertex is determined for each event by a weighted fit of all tracks with a $z$ coordinate within 5 cm of the $z$-vertex position of the primary vertex associated with the trigger lepton. The tracks used in this fit are required to have been reconstructed in the SVX detector. First all tracks are forced to originate from a common vertex. The position of this vertex is constrained by the transverse beam envelope described above. Tracks that have large impact parameters with respect to this vertex are removed, and the fit is repeated. This procedure is iterated until all tracks are within the required impact parameter requirement. At least five tracks must be used in the determination of the transverse position of the primary vertex or we use the nominal beam-line position. The primary vertex coordinates transverse to the beam direction have an uncertainty in the range 10–35 $\mu$m, depending on the number of tracks and the event topology.

The reconstruction of the $B$ decay point (referred to below as the secondary vertex) in the trigger-lepton jet is based on the technique developed to identify jets formed by $b$ quarks coming from $t$ quark decay [12]. Some modifications to this technique were necessary to maintain good efficiency for reconstructing the $B$ hadron decay point in our data sample, since the $B$ hadrons in this sample have substantially lower $p_T$ than the $B$ hadrons from top quark decay. The search for a secondary vertex in the trigger-lepton jet is a two-stage process. In both stages, tracks in the jet are selected for reconstruction of a secondary vertex based on the significance of their impact parameter with respect to the primary vertex, $d_0/\sigma_{d_0}$, where $\sigma_{d_0}$ is the estimate of the uncertainty on $d_0$. The uncertainty $\sigma_{d_0}$ includes contributions from both the primary vertex and the track parameters. The first stage requires at least three candidate tracks for the reconstruction of the secondary vertex. The trigger lepton is always included as a candidate, whether or not it satisfies the $d_0/\sigma_{d_0}$ requirement. Tracks consistent with coming from the decay $K_S^0\rightarrow\pi^+\pi^-$ or $\Lambda^0\rightarrow p\pi^-$ are not used as candidate tracks. Two candidate tracks are constrained to pass through the same space point to form a seed vertex. If at least one additional candi-

date track is consistent with intersecting this seed vertex, then the seed vertex is used as the secondary vertex. If the first stage is not successful in finding a secondary vertex, the second stage is attempted. More stringent track requirements (on $d_0/\sigma_{d_0}$ and $p_T$, for example) are imposed on the candidate tracks. All candidate tracks satisfying these stricter criteria are constrained to pass through the same space point to form a seed vertex. This vertex has an associated $\chi^2$. Candidate tracks that contribute too much to the $\chi^2$ are removed, and a new seed vertex is formed. This procedure is iterated until a seed vertex remains that has at least two associated tracks and an acceptable value of $\chi^2$. The trigger lepton is one of the tracks used to determine the trigger-lepton jet secondary vertex in 96% of the events.

The decay length of the secondary vertex $L_{xy}$ is the projection of the two-dimensional vector pointing from the primary vertex to the secondary vertex on the jet axis (defined by the sum of all the momenta of the tracks included in the jet); if the cosine of the angle between these two vectors is positive (negative), then $L_{xy}$ is positive (negative). Secondary vertices from the decay of $B$ hadrons are expected to have positive $L_{xy}$, while negative $L_{xy}$ vertices usually result from random combinations of mismeasured tracks. To reduce the background from these false vertices, we require $|L_{xy}/\sigma_{L_{xy}}|>2.0$, where $\sigma_{L_{xy}}$ is the estimated uncertainty in $L_{xy}$. We require a secondary vertex to be associated with the trigger-lepton jet. This requirement leaves us with 243 800 events: 114 665 from the electron data sample and 129 135 from the muon data sample. The fraction of events with $L_{xy}<0$ is 4.5% in the electron data sample and 5.7% in the muon data sample. For reasons we discuss later, only events with $L_{xy}>0$ are used in the determination of $\Delta m_d$ and the study of the performance of the flavor tags. The distribution of the number of jets with total transverse momentum $p_T>5$ GeV/$c$ is shown in the upper plot of Fig. 1. Approximately 60% of the events contain a second jet in addition to the trigger-lepton jet. The lower plot in Fig. 1 shows the difference in azimuth between the trigger-lepton jet and the jet with the highest $p_T$ in these events. A large fraction of these jets are back-to-back with the trigger-lepton jet as expected from the lowest-order processes that produce $b\bar{b}$ pairs. We search for secondary vertices in the other jets in the events as well. If an additional secondary vertex is found in one of these other jets, we classify this event as a ''double-vertex'' event. If only the single secondary vertex associated with the trigger-lepton jet is found, this event is classified as a ''single-vertex'' event. The distinction between single-vertex and double-vertex events is important in applying the jet-charge flavor tag as described below.

### D. Determination of the *B* hadron flavor

The next step in the analysis is to identify the flavor at production of the $B$ hadron that produced the trigger lepton. We accomplish this by identifying the flavor of the other $B$ hadron produced in the collision. We refer to this other $B$ hadron as the ''opposite $B$'' in the text below. We first search for an additional lepton coming from the semileptonic

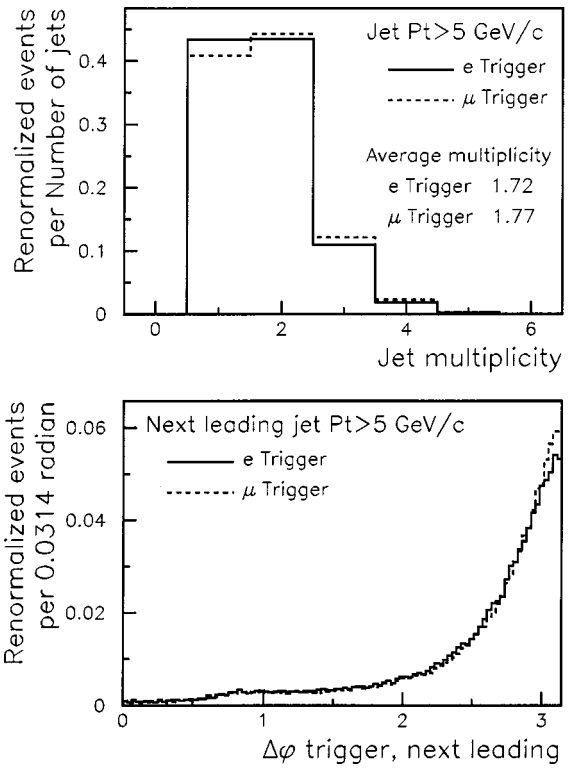


FIG. 1. Jet distributions from the inclusive lepton data samples after the trigger lepton has been associated with a secondary vertex. The upper figure shows the number of jets with transverse momentum $p_t>5$ GeV/$c$ per event. Approximately 60% of the events have more than one jet. The lower figure shows the separation in azimuth of the trigger-lepton jet and the jet with the largest $p_t$ in these events.

decay of this opposite $B$. Because the $p_T$ of this lepton is not biased by the trigger, it is typically much smaller than the $p_T$ of the trigger lepton, so we call this method of flavor identification the ''soft-lepton tag'' or SLT. The soft lepton can be either an electron or a muon. The lepton selection criteria are similar to the selection criteria described in Sec. III A and Ref. [12], with additional selection criteria that use $dE/dx$, and pulse height in the CPR and CES. The soft lepton must have a track with $p_T>2$ GeV/$c$, and the invariant mass of the soft lepton and the trigger lepton must be greater than 5 GeV/$c^2$. This requirement removes soft leptons coming from sequential semileptonic decays of charm particles produced in the decay of the $B$ hadron producing the trigger lepton. The lepton identification criteria restrict the acceptance of the soft leptons to a pseudorapidity of $|\eta|<1.0$, where $\eta=-\ln[\tan(\theta/2)]$. Approximately 5.2% of the 243 800 events contain a soft lepton candidate. If a soft lepton is not found, we try to identify the jet produced by the opposite $B$. We calculate a quantity called the jet charge $Q_{\rm jet}$ of this jet:

$$Q_{\rm jet}=\frac{\sum_i q_i\cdot(\vec{p}_i\cdot\hat{a})}{\sum_i \vec{p}_i\cdot\hat{a}}, \tag{3.1}$$

where $q_i$ and $\vec{p}_i$ are the charge and momentum of the $i$th track in the jet and $\hat{a}$ is a unit vector defining the jet axis. For $b$-quark jets, the sign of the jet charge is on average the same as the sign of the $b$ quark that produced the jet, so the sign of the jet charge may be used to identify the flavor at production of the $B$ hadron producing the trigger lepton. If a second jet in the event other than the trigger-lepton jet has a secondary vertex, then we use this jet to calculate the jet charge. Double-vertex events with a jet-charge flavor tag are referred to as JCDV events. If only the trigger-lepton jet contains a secondary vertex, we search for a jet with $\Delta\phi > \pi/2$ with respect to the trigger lepton and $p_T > 5$ GeV/$c$. If there is more than one jet satisfying the above criteria, we choose the jet with the highest $p_T$. Single-vertex events with a jet-charge flavor tag are referred to as JCSV events. Approximately 7.5% of the 243 800 events above are JCDV events and approximately 42% are JCSV events.

## IV. DATA SAMPLE COMPOSITION

The events in our selected data sample come from three sources: $b\bar{b}$ production, $c\bar{c}$ production, and light quark or gluon production. In each event, the trigger lepton may be a true lepton or it may be a hadron that mimics the experimental signature of a lepton (a fake lepton). The secondary vertex in the trigger-lepton jet may be a true vertex due to the decay of heavy flavor ($b$ or $c$) or a random combination of erroneously reconstructed tracks that appear to form a vertex that is displaced from the primary interaction (a fake vertex). Light quark or gluon jets produce false vertices with $L_{xy} > 0$ with equal probability as false vertices with $L_{xy} < 0$. The small fraction ($< 6\%$) of events with $L_{xy} < 0$ indicates that this background is small. In the analysis, we assume that all events come from heavy flavor ($b\bar{b}$ and $c\bar{c}$) production. The probability of a light quark or gluon event producing a fake vertex and a fake lepton is negligible, although in the evaluation of the systematic uncertainties, we take into account the possible effects of a small amount of non-heavy flavor background. Below, we describe how we determine the fraction of our samples that are due to $b\bar{b}$ production, $c\bar{c}$ production, and fake leptons.

### A. Simulation of heavy flavor production and decay

To understand the composition of our data, we use Monte Carlo samples of $b\bar{b}$ and $c\bar{c}$ production. Version 5.6 of the PYTHIA [16] Monte Carlo generator was used to generate high-statistics $b\bar{b}$ and $c\bar{c}$ samples. The $b\bar{b}$ and $c\bar{c}$ pairs are generated through processes of order up to $\alpha_s^2$ such as $gg \to \mathbf{q}\bar{\mathbf{q}}$ and $q\bar{q} \to \mathbf{q}\bar{\mathbf{q}}$, where $\mathbf{q} = b$ or $c$. Processes of order $\alpha_s^3$, such as gluon splitting, where $gg \to gg$ is followed by $g \to \mathbf{q}\bar{\mathbf{q}}$, are not included, but initial and final state gluon radiation is included. The $b$ and $c$ quarks are hadronized using the fragmentation function of Peterson *et al.* [17] with the parameters $\epsilon_b = 0.006$ and $\epsilon_c = 0.06$. The bottom and charm hadrons were decayed using version 9.1 of the CLEO Monte Carlo program QQ [18]. Events with a lepton with $p_T > 6$ GeV/$c$ were accepted based on an efficiency parametrization [19] of the CFT trigger that depends on the lepton $p_T$. The accepted events were passed through a simulation of the CDF detector that is based on parametrizations and simple models of the detector response that are functions of the particle kinematics. After the simulation of the CDF detector, the Monte Carlo events were treated as if they were real data.

### B. Sources of trigger electrons

The trigger electrons in the sample can come from three sources: heavy flavor decay ($b \to e$, $b \to c \to e$, and $c \to e$), photon conversion ($\gamma \to e^+e^-$ or $\pi^0 \to \gamma e^+e^-$), or hadrons that fake the electron signature in the detector. The contribution from heavy flavor decay is discussed in Sec. IV D. We attempt to identify and reject photon conversions by searching for the partner of the trigger electron. We search for an oppositely charged track that forms a good, zero opening angle vertex with the trigger electron. The $dE/dx$ of this track, as measured in the CTC, must be consistent with the electron hypothesis. We removed 2% of the electron trigger sample that was identified as photon conversions. We estimate that about 1% of the remaining events contain a trigger electron from a photon conversion that was not identified. To determine the fraction of events that contain a hadron that fakes an electron, we fit the trigger-electron $dE/dx$ spectrum for its $e$, $\pi$, $K$, and $p$ content. We found the non-electron fraction of the sample to be $(0.6 \pm 0.5)\%$, where the uncertainty is statistical only. Since this background is small, we neglect it in the remainder of the analysis.

### C. Sources of trigger muons

The trigger muons in the sample can come from heavy flavor decay ($b \to \mu$, $b \to c \to \mu$, and $c \to \mu$), $\pi$ and $K$ decay, and from hadrons that penetrate the absorbing material in front of the muon chambers. The contribution from heavy flavor decay is discussed in Sec. IV D. To study the properties of fake muon events, we used a control sample of events that only required a high $p_T$ CFT track in the trigger. The trigger track was treated like a trigger lepton, and the jet containing the trigger track was required to contain a secondary vertex. The $L_{xy}$ distribution of the control sample was very similar to the heavy flavor Monte Carlo $L_{xy}$ distributions and the $L_{xy}$ of the signal data samples. We conclude from this comparison that due to the secondary vertex requirement most of the fake muon events in the data are events from heavy flavor production. As described in Appendix B, we estimate the fraction of events with a fake trigger muon whose dilution is zero by comparing the flavor tagging performance of the $e$ and $\mu$ trigger data. The estimated fraction of events with fake muons that have zero dilution is $(12 \pm 6)\%$.

### D. Fraction of data sample due to heavy flavor production and decay

We determine the fraction of events in the data due to $b\bar{b}$ and $c\bar{c}$ production using two kinematic quantities: the trigger

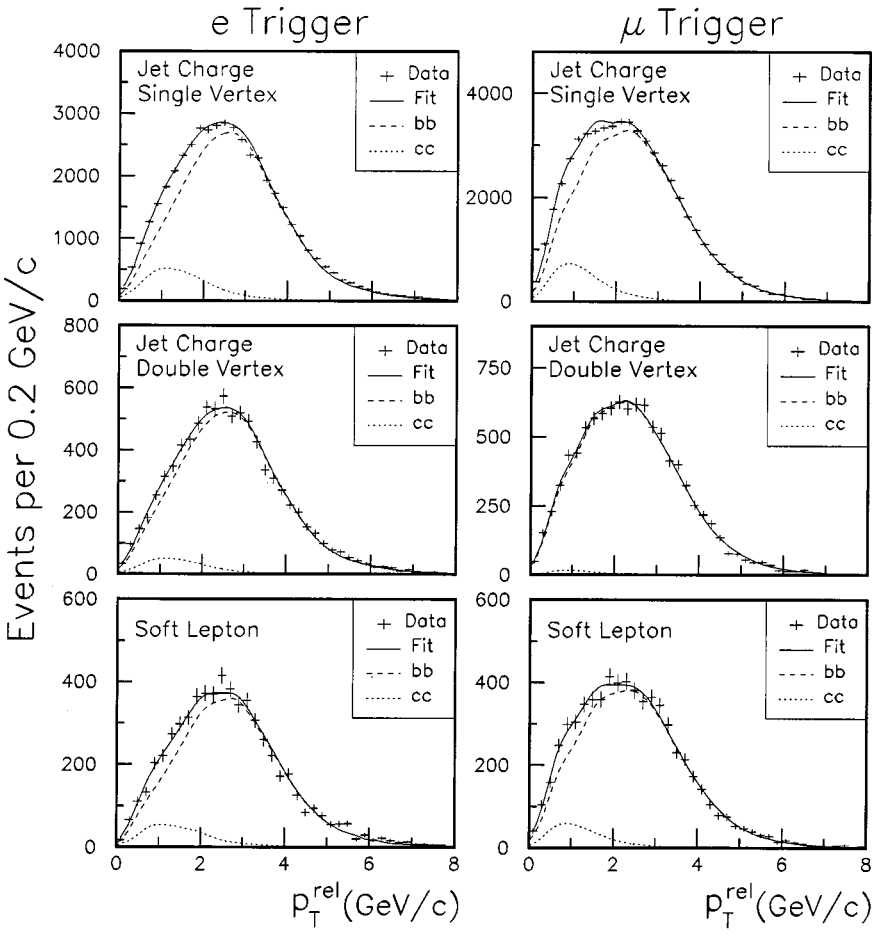


FIG. 2. The sample composition fits using $p_T^{\mathrm{rel}}$. The left hand plots are for the electron data and the right hand plots are for the muon data. The fit values for the fraction of events from $b\bar{b}$ production are given in Table I.

lepton $p_T^{\mathrm{rel}}$ and the invariant mass $m^{\mathrm{cl}}$ of the cluster of secondary vertex tracks. The quantity $p_T^{\mathrm{rel}}$ is defined as the magnitude of the component of the trigger-lepton momentum that is perpendicular to the axis of the trigger-lepton jet. The trigger lepton is removed from the jet, and the jet axis is recalculated to determine $p_T^{\mathrm{rel}}$. To calculate $m^{\mathrm{cl}}$, we assign the pion mass to all of the tracks used to form the secondary vertex (except the trigger lepton). We include the trigger lepton even if it is not attached to the secondary vertex. These kinematic quantities are effective in discriminating between $b\bar{b}$ and $c\bar{c}$ events because of the significant mass difference between the hadrons containing $b$ and $c$ quarks ($\approx 3$ GeV/$c^2$).

Template $p_T^{\mathrm{rel}}$ and $m^{\mathrm{cl}}$ distributions were obtained from the $b\bar{b}$ and $c\bar{c}$ Monte Carlo samples. The $p_T^{\mathrm{rel}}$ and $m^{\mathrm{cl}}$ distributions for the data were fit to the sum of the $b\bar{b}$ and $c\bar{c}$ Monte Carlo templates, where the normalization for each template was a free parameter. The $e$ and $\mu$ trigger data were fit separately, and the data for each trigger were divided according to flavor tag. The three categories were soft lepton (SLT), jet-charge single vertex (JCSV), and jet-charge double vertex (JCDV). The results of the $m^{\mathrm{cl}}$ and $p_T^{\mathrm{rel}}$ fits were averaged to obtain the nominal values for the fraction of events from $b\bar{b}$ production ($F_{b\bar{b}}$). The fits are shown in Fig. 2 and Fig. 3, and Table I gives the nominal values of $F_{b\bar{b}}$ for the $e$ and $\mu$ trigger data. The data are mostly ($>90\%$) from $b\bar{b}$ production.

## V. METHOD OF MEASURING THE FLAVOR TAG $\epsilon D^2$ AND $\Delta m_d$

As outlined in the Introduction, to measure $\Delta m_d$ we compare the flavor of the $B^0$ meson when it was produced to the flavor of the $B^0$ meson when it decays as a function of the proper decay time of the meson.

### A. Reconstruction of the *B* proper decay time *t*

To reconstruct the time of decay in the $B$ rest frame ($t$), we must combine the two-dimensional decay length ($L_{xy}$) with the component of the $B$ momentum in the $x$-$y$ plane ($p_T^B$). The proper time is

$$t = \frac{L_{xy} m_B}{c p_T^B} \tag{5.1}$$

where $m_B$ is the mass of the $B^0$ and $c$ is the speed of light. The proper decay length is the proper time multiplied by the speed of light ($ct$). We do not observe all of the decay products of the $B$: the neutrino from the semileptonic decay is not detected, as well as other neutral decay products and charged

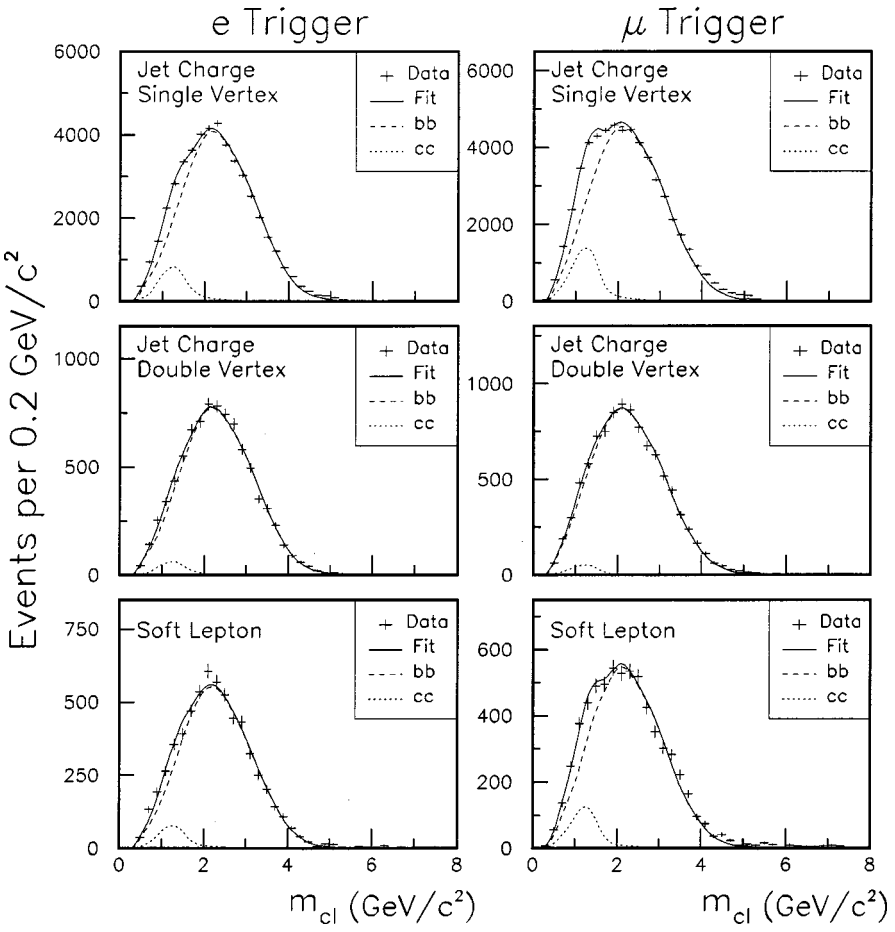


FIG. 3. The sample composition fits using $m_{\rm cl}$. The left hand plots are for the electron data and the right hand plots are for the muon data. The fit values for the fraction of events from $b\overline{b}$ production are given in Table I.

decay products that may not have been associated with the secondary vertex. This means that $p_T^B$ is not known and must be estimated based on observed quantities and the $b\overline{b}$ Monte Carlo samples.

The momentum in the transverse plane of the cluster of secondary vertex tracks $p_T^{\rm cl}$ and $m^{\rm cl}$ are the observed quantities used in the estimation of $p_T^B$. The trigger lepton is included in the calculation of $p_T^{\rm cl}$ and $m^{\rm cl}$, even if it is not attached to the secondary vertex, since we assume that it is a $B$ decay product. The estimate of the $B$ hadron transverse momentum $p_T^{B'}$ for an event is

$$p_T^{B'} = \frac{p_T^{\rm cl}}{\langle K \rangle} \tag{5.2}$$

where $\langle K \rangle$ is the mean of the distribution of $K = p_T^{\rm cl}/p_T^B$ determined with the $b\overline{b}$ Monte Carlo samples. Figure 4 shows $K$ distributions for $m^{\rm cl} < 1.5$ GeV/$c^2$ and $m^{\rm cl} > 3.0$ GeV/$c^2$ as well as for $p_T^{\rm cl} < 11$ GeV/$c$ and $p_T^{\rm cl} > 17$ GeV/$c$. For higher $m^{\rm cl}$ and $p_T^{\rm cl}$ values, the $K$ distribution has a higher mean and a narrower width: a larger fraction of the $B$ momentum is observed so the observed $p_T^{\rm cl}$ is a more precise estimate of the $B$ momentum. To take into account the $m^{\rm cl}$ and $p_T^{\rm cl}$ dependence of the $K$ distribution, we bin the data in four ranges of $m^{\rm cl}$ and $p_T^{\rm cl}$ for a total of 16 $K$ distributions. Different sets of $K$ distributions are used for the $e$ and $\mu$ trigger data.

Figure 5 shows the reconstructed proper decay length ($ct$) distributions for the $e$ and $\mu$ trigger data. The plots of the data are compared to the expected shape from $b\overline{b}$ and $c\overline{c}$ production, where the $b\overline{b}$ and $c\overline{c}$ distributions were combined using $F_{b\overline{b}}$ in Table I and setting the fraction of $c\overline{c}$

TABLE I. The fraction of events from $b\overline{b}$ production $F_{b\overline{b}}$ for the $e$ and $\mu$ trigger data. The first two columns give the result for $F_{b\overline{b}}$ from fitting the $p_T^{\rm rel}$ and $m^{\rm cl}$ spectra to a linear combination of $b\overline{b}$ and $c\overline{c}$ templates. The error in the first two columns is statistical only. The last column gives the average of the $p_T^{\rm rel}$ and $m^{\rm cl}$ results. The error in the average takes into account the difference in the $p_T^{\rm rel}$ and $m^{\rm cl}$ fit results as a systematic error. The fraction of events from $c\overline{c}$ production is given by $F_{c\overline{c}} = 1 - F_{b\overline{b}}$.

| Sample | $p_T^{\rm rel}$ fit | $m^{\rm cl}$ fit | Average value |
|---|---|---|---|
| JCSV($e$) | (89.6±0.6)% | (92.2±0.5)% | (90.9±1.3)% |
| JCDV($e$) | (94.5±1.5)% | (96.7±1.0)% | (95.6±1.5)% |
| SLT($e$) | (91.3±1.7)% | (94.4±1.5)% | (92.9±1.7)% |
| JCSV($\mu$) | (90.1±0.5)% | (89.0±0.5)% | (89.6±1.3)% |
| JCDV($\mu$) | (98.7±1.3)% | (97.6±1.2)% | (98.2±1.3)% |
| SLT($\mu$) | (92.8±1.6)% | (91.5±1.4)% | (92.2±1.6)% |

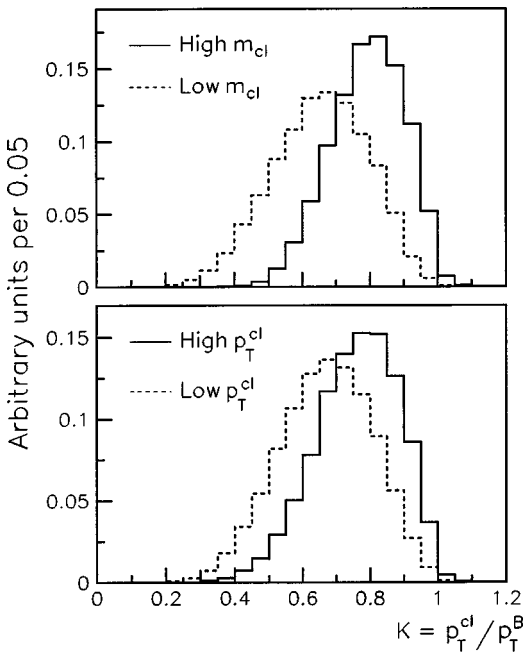


FIG. 4. The observed momentum fraction, which is defined as $p_T^{\rm cl}/p_T^B$. The top plot shows two ranges of cluster mass: $m^{\rm cl}<1.5$ GeV/$c^2$ (dashed line) and $m^{\rm cl}>3.0$ GeV/$c^2$ (solid line). The bottom plot shows two ranges of cluster transverse momentum: $p_T^{\rm cl}<11$ GeV/$c$ (dashed line) and $p_T^{\rm cl}>17$ GeV/$c$ (solid line). The plots were obtained from the $e$-trigger $b\bar{b}$ Monte Carlo sample.

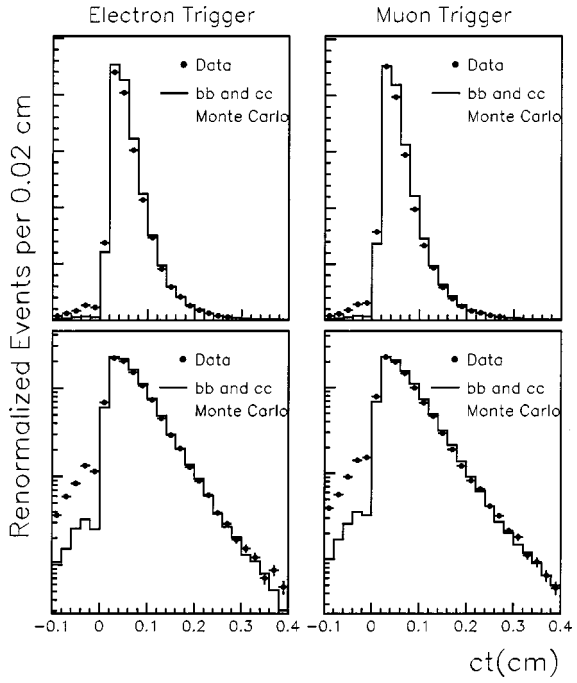


FIG. 5. The reconstructed proper decay length $ct$ for the $e$ and $\mu$ trigger data. The points are the data. The solid histogram is a combination of $b\bar{b}$ and $c\bar{c}$ Monte Carlo sample with the relative fractions given in Table I. All distributions are normalized to unit area. The upper plots show the data on a linear scale while the lower plots show it on a logarithmic scale.

events to $F_{c\bar{c}}=1-F_{b\bar{b}}$. The lack of events near $ct=0$ is due to the transverse decay length significance requirement $|L_{xy}/\sigma_{L_{xy}}|>2$. The exponential fall-off of the data in $ct$ agrees with the Monte Carlo prediction. There is, however, an excess of events with $ct<0$ in the data. This excess is due in part to backgrounds and higher-order processes not included in the Monte Carlo simulation. These backgrounds include electrons from photon conversions and fake muons. The higher-order processes include gluon splitting to $b\bar{b}$ pairs, which can produce a pair of $B$ hadrons that are close in $\Delta R$. In these events, the decay products of both $B$ hadrons may be included in the same jet. This leads to secondary vertices that include tracks from both $B$ hadrons, resulting in a specious measurement of $L_{xy}$ that may be positive or negative. To verify this, we generated a sample of $b\bar{b}$ events using the ISAJET [20] event generator, which includes gluon splitting. This sample showed an increased fraction of reconstructed vertices with negative $L_{xy}$.

### B. Determination of the *B* flavor at decay

The flavor of the $B$ hadron associated with the trigger lepton at the time of decay is identified by the trigger-lepton charge, assuming the lepton is from a semileptonic $B$ decay. A $B$ hadron that contains an anti-$b$ quark ($\bar{b}$) will give a positively charged lepton in a semileptonic decay. The trigger lepton can also originate from the decay of a charmed hadron produced in the decay of the $B$ hadron, e.g. $B\rightarrow DX$, $D\rightarrow l^-X$, which produces ''wrong-sign'' trigger leptons, or $B\rightarrow J/\psi X$, $J/\psi\rightarrow l^+l^-$, which produces both wrong-sign and right-sign trigger leptons. We refer to trigger leptons from these sources as sequential leptons. The Monte Carlo $b\bar{b}$ sample is used to determine the fraction of trigger leptons, $f_{\rm seq}$, from these sequential decays. We find $f_{\rm seq}$ is 9.4% in the electron sample and 13.6% in the muon sample. Approximately 75% of these sequential decays, i.e., 7.0% and 10.2%, produce wrong-sign leptons with the charge opposite to the charge from direct semileptonic decay. We assign a systematic uncertainty of 25% of its value to the fraction of sequential leptons, based on uncertainties on the branching fractions included in the CLEO Monte Carlo program QQ and on measurements of these branching fractions at the $\Upsilon(4S)$ and the $Z^0$ resonance.

### C. Determination of the *B* flavor at production

To determine the flavor of the trigger lepton $B$ at the time of production, we attempt to identify the flavor of the other $B$ in the event, and assume that the original flavor of the trigger lepton $B$ is opposite that of the other $B$. As described previously, we use two methods to obtain the flavor of the other $B$ in the event: soft-lepton tagging (SLT) and jet-charge tagging (JCT). The jet-charge tag has two subclasses: jet-charge double vertex (JCDV) and jet-charge single vertex (JCSV). The soft-lepton method is the most effective (i.e., has the highest probability of producing a correct tag), but least efficient method. The jet-charge methods are less effective, but more efficient. The presence of a secondary vertex in the jet used for the jet charge greatly enhances its effectiveness.

#### *1. Quantifying the statistical power of the flavor tags*

We quantify the statistical power of the flavor tagging methods with the product $\epsilon D^2$, where $\epsilon$ is the efficiency for applying the flavor tag, and $D$ is the dilution, which is related to the probability that the tag is correct ($P_{\rm tag}$) by

$$D = 2P_{\rm tag} - 1. \tag{5.3}$$

An equivalent expression for $D$ is given by

$$D = \frac{N_T - N_M}{N_T + N_M} \tag{5.4}$$

where $N_T$ ($N_M$) is the number of correctly (incorrectly) tagged events. We measure $\epsilon D^2$ in our data. To illustrate the statistical significance of the product $\epsilon D^2$, we discuss an asymmetry measurement with two types of events, $a$ and $b$, where the flavor tagging method identifies whether the event is of type $a$ or type $b$. Type $a$ and type $b$ could be ''mixed'' and ''unmixed'' decays of a neutral $B$ meson, for example. The measured asymmetry $A_{\rm meas}$ is

$$A_{\rm meas} = \frac{N_a - N_b}{N_a + N_b}, \tag{5.5}$$

where $N_a$ and $N_b$ are the number of events that are tagged as type $a$ and type $b$, respectively. The true asymmetry $A$ is

$$A = \frac{N_a^0 - N_b^0}{N_a^0 + N_b^0}, \tag{5.6}$$

where $N_a^0$ and $N_b^0$ are the true number of events of type $a$ and type $b$, respectively, in the sample. The efficiency is

$$\epsilon = \frac{N_a + N_b}{N_a^0 + N_b^0}. \tag{5.7}$$

The true asymmetry is related to the measured asymmetry by

$$A = \frac{1}{D} A_{\rm meas}, \tag{5.8}$$

and the statistical uncertainty on the true asymmetry is

$$\sigma_A = \sqrt{\frac{1 - D^2 A^2}{\epsilon D^2 T}}, \tag{5.9}$$

where $T$ is the total number of events in the sample $T = N_a^0 + N_b^0$. The statistical power of different flavor tagging methods varies as $\epsilon D^2$.

#### *2. Measuring the dilution of the flavor tags*

We measure the dilution of the flavor tags from our data sample. We start by defining a raw dilution, $D_{\rm raw}$:

$$D_{\rm raw} = \frac{N_{\rm OS} - N_{\rm SS}}{N_{\rm OS} + N_{\rm SS}}, \tag{5.10}$$

where $N_{\rm OS}$ and $N_{\rm SS}$ are the number of opposite-sign and same-sign events, respectively. The sign comparison is between the charge of the trigger lepton and either the charge of the soft lepton or the sign of the jet charge. If the charge of the trigger lepton unambiguously identified the flavor at production of the $B$ hadron, then $D_{\rm raw}$ would be equal to the true dilution $D$ of the flavor tag. All same-sign events would result from the flavor tag being incorrect. However, since some same-sign events result from events with a trigger lepton from a $B$ meson that mixed, events with a trigger lepton from sequential decay, events with a fake trigger lepton, or events from $c\overline{c}$ production, $D_{\rm raw}$ is an underestimate of the true dilution of the flavor tag. Nevertheless, the true dilution is approximately related to $D_{\rm raw}$ by a scale factor $N_D$:

$$D = N_D D_{\rm raw}. \tag{5.11}$$

The form of Eq. (5.11) is derived in Appendix A. We use this estimation of the true dilution to estimate the probability that the flavor tag is correct on an event-by-event basis:

$$P_{\rm tag} = \frac{1}{2}(1 + N_D D_{\rm raw}). \tag{5.12}$$

This probability is used in the measurement of $\Delta m_d$ as described in Sec. V D. The dilution normalization $N_D$ is determined simultaneously with $\Delta m_d$.

#### *3. Dilution for the soft-lepton tag*

To maximize the effectiveness of the soft-lepton flavor tag, the data are binned in the $p_T^{\rm rel}$ of the soft lepton. The $p_T^{\rm rel}$ of the soft lepton is defined in the same way as the $p_T^{\rm rel}$ of the trigger lepton. The same-sign and opposite-sign soft-lepton $p_T^{\rm rel}$ distributions are shown in Fig. 6, where the sign comparison is between the trigger-lepton charge and soft-lepton charge. The $p_T^{\rm rel} < 0$ bin is for the case where the soft lepton is the only track in the jet, so that $p_T^{\rm rel} = 0$. If neither $B$ decayed in a mixed state and if both leptons are from semileptonic decay, the charge of the trigger lepton would be opposite the charge of the soft lepton. Figure 7 shows the raw dilution $D_{\rm raw}$ for the soft-lepton tagged events. The raw dilution is derived from the number of same-sign and opposite-sign events in each bin of $p_T^{\rm rel}$. The dilution is lower for low $p_T^{\rm rel}$ because fake leptons and leptons from sequential semileptonic decay tend to have relatively low $p_T^{\rm rel}$ values. The $p_T^{\rm rel}$ dependence of $D_{\rm raw}$ was parametrized using the form

$$D_{\rm raw}(p_T^{\rm rel}) = A(1 - e^{-p_T^{\rm rel} + B}), \tag{5.13}$$

where $A$ and $B$ are parameters determined from the data. The average raw dilution is used for isolated soft leptons that have no measurement of $p_T^{\rm rel}$. The form of Eq. (5.13) is empirical and was found to describe the shape of $D_{\rm raw}$ as a function of $p_T^{\rm rel}$ well in the Monte Carlo samples. Parameters $A$ and $B$ are measured separately for the $e$ and $\mu$ trigger data because the fraction of trigger leptons from sequential decay and the trigger lepton purity are different for the $e$ and $\mu$ data, which affects the raw dilution. Parameters $A$ and $B$ are

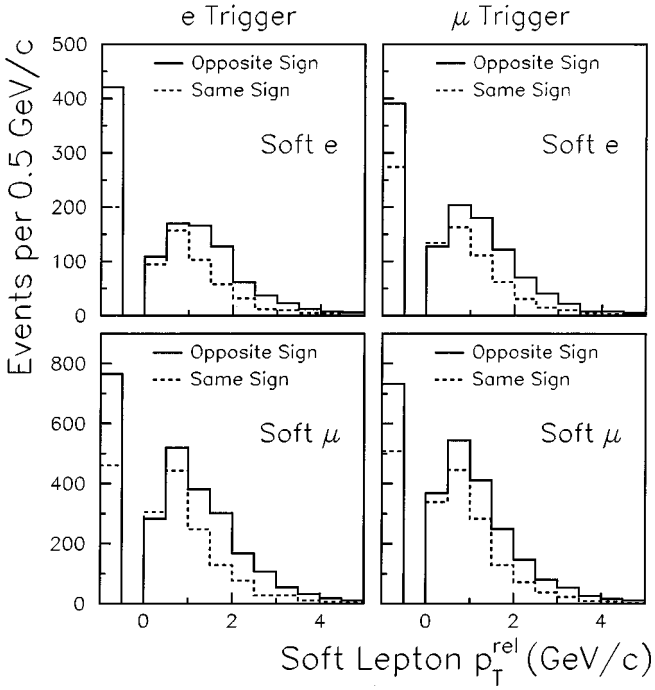


FIG. 6. Distributions of soft-$e$ and soft-$\mu$ $p_T^{\rm rel}$ for $e$-trigger and $\mu$-trigger events. The solid (dashed line) distributions are for events where the charge of the soft and trigger leptons have opposite (like) sign. The bin below 0 is for events where the soft lepton was isolated.

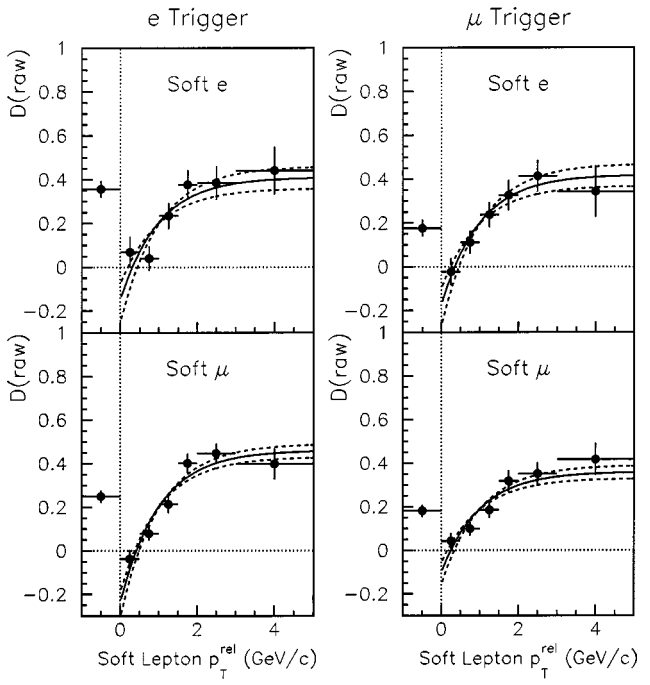


FIG. 7. Soft-$e$ and soft-$\mu$ tag raw dilution as a function of soft-lepton $p_T^{\rm rel}$ for the $e$ and $\mu$ trigger data. The solid curve is the parametrization used for calculating the expected raw dilution on an event-by-event basis based on the soft-lepton $p_T^{\rm rel}$. The dashed curves show the variation used in the evaluation of the systematic uncertainty in the raw dilution parameterization.

also measured separately for the soft-$e$ and soft-$\mu$ tags because the fractions of fake soft leptons may be different for soft electrons and soft muons. The fitted values of $A$ and $B$ and the average raw dilution for isolated (no $p_T^{\rm rel}$) soft leptons for soft-$e$ and soft-$\mu$ tags in the $e$ and $\mu$ trigger data are listed in Table II.

The values of $A$ and $B$ determined from the data are assumed to describe the SLT raw dilution as a function of $p_T^{\rm rel}$ for $b\bar{b}$ events. This is only an approximation since a small fraction (less than 10%) of the data are $c\bar{c}$ events. A $c\bar{c}$ event in which $c\to l^+\nu s$ and $\bar{c}\to l^-\bar{\nu}\bar{s}$ can produce opposite-sign events in which one of the leptons is associated with a secondary vertex, and the other lepton produces a soft-lepton tag. The soft-lepton tags in $c\bar{c}$ events have a much softer $p_T^{\rm rel}$ spectrum than soft-lepton tags in $b\bar{b}$ events. The Monte Carlo simulation demonstrates that $c\bar{c}$ events affect the values of $A$ and $B$ by an amount less than the statistical uncertainties in the fitted values of $A$ and $B$. The effects of the approximation above are accounted for since the values of $A$ and $B$ are varied by their statistical uncertainties in the determination of the systematic uncertainties on $\Delta m_d$ and the dilution normalization parameters.

#### *4. Dilution for the jet-charge tag*

Figure 8 shows the jet charge distributions for single-vertex and double-vertex events. The data have been divided into events with a positively or negatively charged trigger lepton ($l$). There is an anticorrelation between the sign of the jet charge and the trigger-lepton charge on average. The degree of separation between the $l^+$ and $l^-$ distributions is related to the raw dilution of the jet-charge flavor tag, shown in Fig. 9 as a function of the magnitude of the jet charge $|Q_{\rm jet}|$. For double-vertex events, the presence of the second secondary vertex increases the probability that the jet selected for the calculation of the jet charge does in fact contain the other $B$ in the event. This translates into a significantly higher raw dilution for double-vertex events.

The $|Q_{\rm jet}|$ dependence of $D_{\rm raw}$ is used to predict the probability that the jet-charge tag is correct on an event-by-event basis, just as $p_T^{\rm rel}$ is used for soft leptons. The $|Q_{\rm jet}|$ dependence of $D_{\rm raw}$ in the data in Fig. 9 was parametrized with the form

TABLE II. Fitted values for the SLT raw dilution parametrization constants ($A$ and $B$) and the raw dilution for isolated soft leptons (no-$p_T^{\rm rel}$) for soft $e$ and $\mu$ tags in the $e$ and $\mu$ trigger data. The errors are statistical. The SLT raw dilution is parametrized as a function of the soft lepton $p_T^{\rm rel}$ with the functional form $D_{\rm raw}(p_T^{\rm rel}) = A(1-e^{-p_T^{\rm rel}+B})$ where $p_T^{\rm rel}$ is in GeV/$c$.

| | $e$-trigger | | $\mu$-trigger | |
|---|---|---|---|---|
| | Soft-$e$ | Soft-$\mu$ | Soft-$e$ | Soft-$\mu$ |
| $A$ | $0.41\pm0.05$ | $0.46\pm0.03$ | $0.42\pm0.05$ | $0.36\pm0.03$ |
| $B$ | $0.31\pm0.13$ | $0.43\pm0.06$ | $0.35\pm0.11$ | $0.25\pm0.09$ |
| no-$p_T^{\rm rel}$ | $0.36\pm0.04$ | $0.25\pm0.03$ | $0.18\pm0.04$ | $0.18\pm0.03$ |

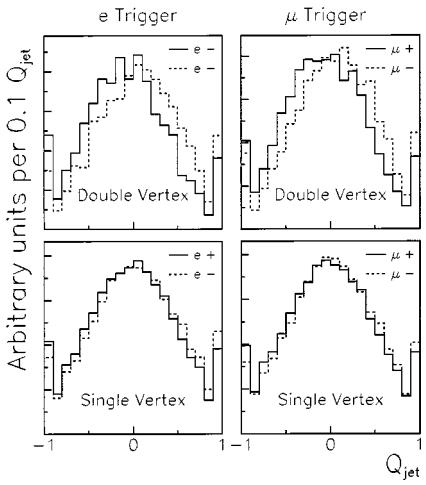


FIG. 8. Jet charge distributions for double (top) and single (bottom) vertex events for the $e$ and $\mu$ trigger data. The data have been divided into events with a positively or negatively charged trigger lepton ($l^+$ or $l^-$). Note that the separation between the $l^+$ and $l^-$ distributions is significantly larger for the double vertex events.

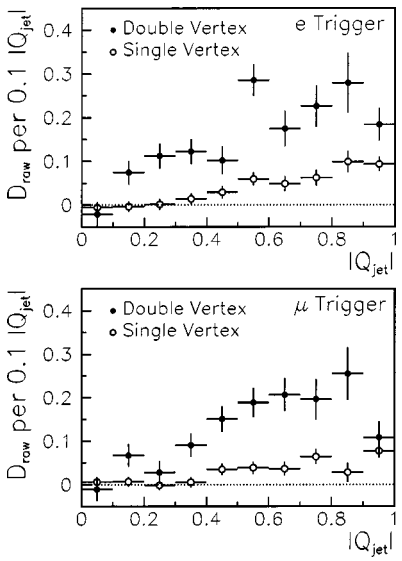


FIG. 9. The raw dilution $D_{\rm raw}$ as a function of absolute jet charge $|Q_{\rm jet}|$ for double and single vertex events in the $e$ and $\mu$ trigger data. Note the significantly higher dilution for double vertex events.

$$D_{\rm raw}(|Q_{\rm jet}|)=|Q_{\rm jet}|D_{\rm max} \tag{5.14}$$

excluding events with $|Q_{\rm jet}|=1$ (the rightmost data point). For events with $|Q_{\rm jet}|=1$, the average $|Q_{\rm jet}|=1$ dilution is used. The slope $D_{\rm max}$ is determined separately for the single-vertex and double-vertex events in the $e$ and $\mu$ trigger data, respectively. These slopes and the average raw dilution for $|Q_{\rm jet}|=1$ are listed in Table III. We use Eq. (5.12), with $D_{\rm raw}$ estimated for each event using Eq. (5.13) for SLT events and Eq. (5.14) for JCT events, in the determination of $\Delta m_d$ to effectively discriminate between high and low quality flavor tags.

### D. Unbinned maximum likelihood fit

We use an unbinned maximum likelihood fit to simultaneously determine $\Delta m_d$ and the dilution normalization $N_D$. The effectiveness ($\epsilon D^2$) of each flavor tag is derived from the measured $\epsilon$, $D_{\rm raw}$, and the dilution normalization ($N_D$) from the fit. The fraction of $B^0$ mesons that decay in a mixed state as a function of the proper time at decay is given by

$$F_{\rm mix}(t)=\frac{1}{2}[1-\cos(\Delta m_d\cdot t)]. \tag{5.15}$$

In a pure $B_d^0$ sample with perfect flavor tagging and proper time resolution, $F_{\rm mix}(t)$ would be equivalent to the fraction of same-sign events, comparing the sign of the flavors at decay and production. If the flavor tag is imperfect, Eq. (5.15) becomes

$$F_{\rm mix}(t)=P_{\rm tag}\frac{1}{2}[1-\cos(\Delta m_d t)] + P_{\rm mistag}\frac{1}{2}[1+\cos(\Delta m_d t)], \tag{5.16}$$

where $P_{\rm tag}$ ($P_{\rm mistag}$) is the probability that the flavor tag is correct (incorrect). Using the relations

$$P_{\rm tag}=\frac{1}{2}(1+N_D D_{\rm raw}), \tag{5.17}$$

$$P_{\rm mistag}=\frac{1}{2}(1-N_D D_{\rm raw}), \tag{5.18}$$

Eq. (5.16) reduces to

$$F_{\rm mix}(t)=\frac{1}{2}[1-N_D D_{\rm raw}\cos(\Delta m_d t)]. \tag{5.19}$$

TABLE III. Constants for the jet-charge tag raw dilution parametrization as a function of $|Q_{\rm jet}|$. The parametrization has the form $D_{\rm raw}=D_{\rm max}|Q_{\rm jet}|$ except for events where $|Q_{\rm jet}|=1$, in which case the average $D_{\rm raw}$ is used.

| | $e$-trigger | | $\mu$-trigger | |
|---|---|---|---|---|
| | JCSV | JCDV | JCSV | JCDV |
| $D_{\rm max}$ | $0.083\pm0.010$ | $0.34\pm0.02$ | $0.060\pm0.009$ | $0.29\pm0.02$ |
| $D_{\rm raw}$, $\lvert Q_{\rm jet}\rvert=1$ | $0.091\pm0.014$ | $0.18\pm0.03$ | $0.074\pm0.014$ | $0.12\pm0.03$ |

TABLE IV. The fixed input parameters used in the fit. The first column lists the parameters, which are described below. The second column lists the value of the parameter assumed for the fit, with an error in this parameter, if appropriate. The third column lists the variation of the parameter for the purposes of evaluating the systematic errors on $\Delta m_d$ and $N_D$; $\pm 1\sigma$ means that the parameter was varied by the error listed in the second column. Finally the fourth column lists the source of the parameter. The fixed input parameters are the $B$ hadron lifetimes ($\tau_i$), the $B_s^0$ mass difference ($\Delta m_s$), the relative $B$ hadron production fractions [$f(\bar{b} \to X)$], the fraction of trigger leptons from $b\bar{b}$ sources other than direct $B$ decay ($f_{\rm seq}$), the flavor tag dilution value for $c\bar{c}$ events ($D_{c\bar{c}}$), an effective lifetime for $c\bar{c}$ events ($\tau_{c\bar{c}}$), and the fraction of $\mu$-trigger events where the trigger muon is really a hadron and has a dilution of zero ($F^0_{\rm fake\ \mu}$).

| Parameter | Value | Variation | Source |
|---|---|---|---|
| $\tau_{B^0}$ | $1.56 \pm 0.06$ ps | $\pm 1\sigma$ | [21] |
| $\tau_{B^+}/\tau_{B^0}$ | $1.02 \pm 0.05$ | $\pm 1\sigma$ | [21] |
| $\tau_{B_s^0}$ | $1.61^{+0.10}_{-0.09}$ ps | $\pm 1\sigma$ | [21] |
| $\tau_{\Lambda_b}$ | $1.14 \pm 0.08$ ps | $\pm 1\sigma$ | [21] |
| $\Delta m_s$ | $700\hbar$ ps$^{-1}$ | down to $6.7\hbar$ ps$^{-1}$ | assumption |
| $f(\bar{b} \to B^+)$ | $(37.8 \pm 2.2)\%$ | $\pm 1\sigma$ | [21] |
| $f(\bar{b} \to B^0)$ | $(37.8 \pm 2.2)\%$ | $\pm 1\sigma$ | [21] |
| $f(\bar{b} \to B_s^0)$ | $(11.1^{+2.5}_{-2.6})\%$ | $\pm 1\sigma$ | [21] |
| $f(b \to \Lambda_b)$ | $(13.2 \pm 4.1)\%$ | $\pm 1\sigma$ | [21] |
| $f_{\rm seq}$ | $e$: 9.4% | $\pm 0.25 \times f_{\rm seq}$ | Monte Carlo |
| | $\mu$: 13.6% | $\pm 0.25 \times f_{\rm seq}$ | Monte Carlo |
| JCT $D_{c\bar{c}}/D_{b\bar{b}}$ | 0.5 | 0 to 1 | assumption |
| SLT $D_{c\bar{c}}$ | 0.5 | 0 to 1 | assumption |
| $\tau_{c\bar{c}}$ | $1.53 \pm 0.20$ ps | $\pm 1\sigma$ | fit to $c\bar{c}$ MC |
| $F^0_{\rm fake\ \mu}$ | $(12 \pm 6)\%$ | $\pm 1\sigma$ | $e/\mu$ $D_{\rm raw}$ comparison |

Although $N_D$ and $\Delta m_d$ are correlated, the basic concept is that $N_D$ is determined from the amplitude of the oscillation in the same-sign fraction and $\Delta m_d$ is determined from the frequency.

We determine $\Delta m_d$ and $N_D$ by minimizing [21] the negative logarithmic likelihood:

$$-\ln \mathcal{L} = \sum_i^{n_{\rm SS}} \ln(\mathcal{P}^i_{\rm SS}) + \sum_j^{n_{\rm OS}} \ln(\mathcal{P}^j_{\rm OS}), \tag{5.20}$$

where $\mathcal{P}_{\rm SS}$ is the probability density for events that are tagged as same-sign, and $\mathcal{P}_{\rm OS}$ is the probability density for events that are tagged as opposite-sign. Each event has three inputs into the likelihood:

(1) the assignment as same sign or opposite sign, which is based on the comparison of the sign of the SLT or JCT flavor tag with the charge of the trigger lepton,

(2) the estimated probability that the SLT or JCT flavor tag is correct, using Eq. (5.12), with $D_{\rm raw}$ from Eq. (5.13) for the SLT flavor tag or from Eq. (5.14) for the JCT flavor tag,

(3) the decay distance $L_{xy}$.

In addition to the above three inputs, we use $p_T^{\rm cl}$ and $m^{\rm cl}$ to select the $K$ distribution that is used in the determination of the reconstructed proper decay distance. The construction of the probability densities requires several parameters. These parameters are listed in Table IV.

Both $\mathcal{P}_{\rm SS}$ and $\mathcal{P}_{\rm OS}$ are the sum of several terms. First they have a term for the $B^0$ signal:

$$\mathcal{P}_{\rm OS}(B^0) = \mathcal{P}_{\rm tag}\mathcal{P}_{\rm nomix} + \mathcal{P}_{\rm mistag}\mathcal{P}_{\rm mix}, \tag{5.21}$$

$$\mathcal{P}_{\rm SS}(B^0) = \mathcal{P}_{\rm tag}\mathcal{P}_{\rm mix} + \mathcal{P}_{\rm mistag}\mathcal{P}_{\rm nomix}, \tag{5.22}$$

where $\mathcal{P}_{\rm tag}$ and $\mathcal{P}_{\rm mistag}$ are given by Eqs. (5.17) and (5.18), respectively, and $\mathcal{P}_{\rm nomix}$ and $\mathcal{P}_{\rm mix}$ are given by Eqs. (1.3) and (1.4), respectively. Next there are terms for the other $B$ hadrons, including terms for both $B^+$ and $b$ baryons, as well as a term for $B_s^0$. The terms for $B^+$ are

$$\mathcal{P}_{\rm OS}(B^+) = \mathcal{P}_{\rm tag}\frac{1}{\tau_{B^+}} e^{-t/\tau_{B^+}}, \tag{5.23}$$

$$\mathcal{P}_{\rm SS}(B^+) = \mathcal{P}_{\rm mistag}\frac{1}{\tau_{B^+}} e^{-t/\tau_{B^+}}, \tag{5.24}$$

where $\tau_{B^+}$ is the lifetime of the $B^+$, and $t$ is the proper decay-time. The terms for $b$ baryons are similar, except that $\tau_{B^+}$ is replaced by the lifetime of the $b$ baryons, $\tau_{\rm baryon}$. The terms for $B_s^0$ are similar to the terms for $B^0$, except that $\Delta m_d$

is replaced by $\Delta m_s$, which is assumed to be very large (i.e. beyond our experimental sensitivity) so that these terms effectively look like

$$\mathcal{P}_{\rm OS}(B_s^0)=\mathcal{P}_{\rm SS}(B_s^0)=\frac{1}{2\tau_{B_s^0}}e^{-t/\tau_{B_s^0}}. \qquad (5.25)$$

The values of the lifetimes of the $B$ hadrons and the value of $\Delta m_s$ used in the probability densities are listed in Table IV. Each term for the various $B$ hadrons is multiplied by the expected relative contribution, $f(\bar{b}\to B^0)$, $f(\bar{b}\to B^+)$, $f(\bar{b}\to B_s^0)$, and $f(b\to\text{baryon})$, of these various hadrons to the data sample. The production fractions are renormalized to take into account the different semileptonic branching fractions of the various $B$ hadrons: the semileptonic widths are assumed to be identical, so the semileptonic branching fractions are scaled to agree with the relative lifetimes.

In addition to the terms for direct semileptonic decay, there are terms that take into account the contribution from sequential decays. The fraction of sequential decays $f_{\rm seq}$ is listed in Table IV; 75% of these sequential decays produce leptons with a sign opposite to direct semileptonic decay.

The terms that take into account the contribution from $c\bar{c}$ events are similar to the terms for $B^+$, except that we use an assumed flavor tagging dilution and an effective lifetime $\tau_{c\bar{c}}$. The true flavor tagging dilution is not known *a priori* for both bottom and charm decays. Just as for $B$ decays, we do not consider the Monte Carlo simulation reliable for predicting the JCT or SLT dilution for charm decays, so we use assumed values for the charm dilution and vary them by the maximum possible amount for the systematic uncertainties. For the JCT, we expect the dilution for charm decays to be worse than for bottom decays; therefore we assume $D_{c\bar{c}}/D_{b\bar{b}}=0.5$ for the JCT, and vary $D_{c\bar{c}}/D_{b\bar{b}}$ from 0 to 1 in the evaluation of the systematic errors. The ratio $D_{c\bar{c}}/D_{b\bar{b}}$ is used to rescale the predicted $b\bar{b}$ dilution for the event, based on $|Q_{\rm jet}|$ using Eq. (5.14), to give the predicted $c\bar{c}$ dilution for the event. The SLT dilution for charm decays could be anything from 0 to 1 depending on the fraction of fake soft leptons in $c\bar{c}$ events. Unlike bottom decays, the SLT dilution for charm decays does not fall near $p_T^{\rm rel}=0$ due to soft leptons from sequential decays; therefore we assume $D_{c\bar{c}}=0.5$, independent of $p_T^{\rm rel}$ for the SLT, and vary $D_{c\bar{c}}/D_{b\bar{b}}$ from 0 to 1 in the evaluation of the systematic errors.

The effective lifetime $\tau_{c\bar{c}}=1.53$ ps is determined from the $c\bar{c}$ Monte Carlo samples, where the proper time at decay was reconstructed using the $K$ distributions from the $b\bar{b}$ Monte Carlo samples and Eq. (5.1). The relative fractions of $b\bar{b}$ ($F_{b\bar{b}}$) and $c\bar{c}$ ($F_{c\bar{c}}$), which can be determined from Table I, multiply the terms in the likelihood corresponding to $b\bar{b}$ and $c\bar{c}$ production, respectively. Finally, for the case of the $\mu$-trigger data, a term for fake muons was included with the $B^0$ lifetime and zero dilution. The relative fraction of fake muons $F^0_{\text{fake }\mu}$ (discussed in Appendix B) is listed in Table IV. In this case, $F_{b\bar{b}}$ and $F_{c\bar{c}}$ are scaled by $1-F^0_{\text{fake }\mu}$.

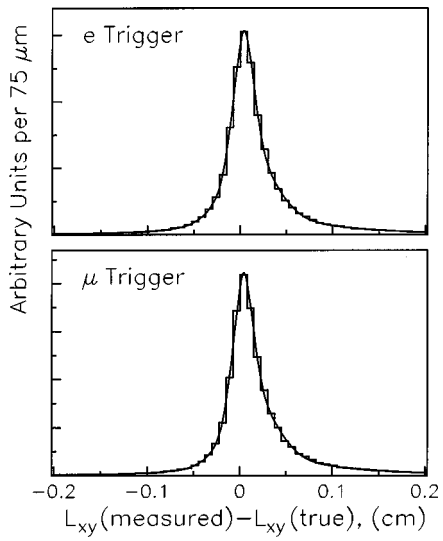


FIG. 10. The transverse decay length resolution functions, defined as the difference between the measured and true $L_{xy}$ in the $b\bar{b}$ Monte Carlo, for the $e$ and $\mu$ trigger data. The distributions were fit to three Gaussians and two exponentials.

The probability densities $P_{\rm SS}(t)$ and $P_{\rm OS}(t)$ are functions of the true proper time at decay $t$. We take into account the experimental resolution of $t$ by convoluting $P_{\rm SS}(t)$ and $P_{\rm OS}(t)$ with $L_{xy}$ and $p_T^{B'}$ resolution functions. Distributions of $\delta L_{xy}\equiv L_{xy}(\text{measured})-L_{xy}(\text{true})$ from the $e$ and $\mu$ trigger $b\bar{b}$ Monte Carlo samples are parametrized with the sum of three Gaussians, a $\delta L_{xy}>0$ exponential, and a $\delta L_{xy}<0$ exponential. The $\delta L_{xy}$ distributions and their parametrizations are shown in Fig. 10 for the $e$ and $\mu$ trigger data. The $K$ distributions, like those shown in Fig. 4, are used as $p_T^{B'}$ resolution functions. The $L_{xy}$ and $p_T^{B'}$ resolution functions describe the $t$ smearing for $b\bar{b}$ events from direct production ($gg\to b\bar{b}$ and $q\bar{q}\to b\bar{b}$). They do not describe backgrounds such as photon conversion events (for the $e$ trigger) or events with a fake trigger muon. They also do not describe $b\bar{b}$ events from gluon splitting ($gg\to gg$ followed by $g\to b\bar{b}$), which tend to have worse $t$ resolution due to secondary vertices that include decay products from both $B$ hadrons. While the total amounts of these backgrounds are reasonably small, they become more important near $ct=0$ and for very large $ct$ values (beyond several $B$ lifetimes). For these reasons, we only use events with $0.02\ \text{cm}<ct<0.30\ \text{cm}$ in the fit for $\Delta m_d$ and the dilution normalization $N_D$.

## VI. FIT RESULTS

The free parameters in the unbinned maximum likelihood fit are the mass difference $\Delta m_d$ and the dilution normalization factors $N_D$. There are six dilution normalization factors:

(1) $N^e_{D,\rm JCSV}$ and $N^\mu_{D,\rm JCSV}$: the dilution normalization factors for the jet-charge flavor tag in the case that the jet does not contain a secondary vertex for the electron-trigger and muon-trigger data samples, respectively.

TABLE V. Results of the maximum likelihood fit for $\Delta m_d$ and the flavor tag dilution normalization factors for the individual flavor taggers separately in the $e$ and $\mu$ trigger data. The first error is statistical and the second is systematic. The evaluation of the systematic errors is discussed later in the text. The dilution normalization factors are given for two cases: $\Delta m_d$ free to float in the fit and $\Delta m_d$ fixed to the 1996 world average [22] ($0.474\hbar$ ps$^{-1}$).

| | SLT | JCSV | JCDV |
|---|---|---|---|
| $e$-trigger | | | |
| $N_D$, $\Delta m_d$ free | $1.66\pm0.12\pm0.18$ | $1.84\pm0.23\pm0.19$ | $1.71\pm0.16\pm0.11$ |
| $N_D$, $\Delta m_d$ fixed | $1.72\pm0.08\pm0.11$ | $1.88\pm0.20\pm0.15$ | $1.76\pm0.13\pm0.09$ |
| $\Delta m_d$ ($\hbar$ ps$^{-1}$) | $0.45\pm0.08\pm0.05$ | $0.42\pm0.09\pm0.03$ | |
| $\mu$-trigger | | | |
| $N_D$, $\Delta m_d$ free | $2.05\pm0.19\pm0.37$ | $2.86\pm0.40\pm0.43$ | $2.52\pm0.28\pm0.25$ |
| $N_D$, $\Delta m_d$ fixed | $2.01\pm0.13\pm0.22$ | $2.41\pm0.29\pm0.39$ | $2.14\pm0.33\pm0.25$ |
| $\Delta m_d$ ($\hbar$ ps$^{-1}$) | $0.50\pm0.09\pm0.05$ | $0.68\pm0.11\pm0.04$ | |

(2) $N^e_{D,\mathrm{JCDV}}$ and $N^\mu_{D,\mathrm{JCDV}}$: the dilution normalization factors for the jet-charge flavor tag in the case that the jet does contain a secondary vertex for the electron-trigger and muon-trigger data samples, respectively.

(3) $N^e_{D,\mathrm{SLT}}$ and $N^\mu_{D,\mathrm{SLT}}$: the dilution normalization factors for the soft-lepton flavor tag for the electron-trigger and muon-trigger data samples, respectively.

To determine the dilution normalization factors needed to calculate the flavor tag $\epsilon D^2$ values (see Sec. VI C), the data are grouped into four subsamples:

(1) $e$-trigger, soft-lepton flavor tag,

(2) $e$-trigger, jet-charge flavor tag,

(3) $\mu$-trigger, soft-lepton flavor tag,

(4) $\mu$-trigger, jet-charge flavor tag.

There is some overlap of events in these four subsamples as some events have both a SLT and a JCT. About 20% of the events with soft-lepton tags did not pass the single-lepton level 2 trigger and came, instead, from a dilepton trigger. In order for the SLT efficiency to be well defined, we require that the SLT events pass the single-lepton trigger in data subsamples 1 and 3, which are used to determine $N^e_{D,\mathrm{SLT}}$, $N^\mu_{D,\mathrm{SLT}}$, and the SLT efficiencies needed for calculating the SLT $\epsilon D^2$.

The fit results for the individual flavor taggers are given in Table V. The dilution normalization factors are given for two cases: $\Delta m_d$ free to float in the fit and $\Delta m_d$ fixed to the world average [22] ($0.474\hbar$ ps$^{-1}$). The value of $\Delta m_d$ is held fixed to the world average because $\Delta m_d$ and the $N_D$ factors are correlated. The correlation coefficients between $\Delta m_d$ and the $N_D$ constants range from 0.55 to 0.81. Fixing $\Delta m_d$ reduces the statistical uncertainty in the dilution normalization constants and removes any bias from statistical fluctuations that pull $\Delta m_d$ high or low. The $N_D$ factors determined with $\Delta m_d$ fixed to the world average are used in the calculation of the flavor tag $\epsilon D^2$ values. The $N_D$ factors in Table V are consistent with our expectations from the composition of the data (see Appendix A).

To determine $\Delta m_d$, we fit all four data subsamples simultaneously. For events with both a SLT and a JCT, we use the SLT because it has significantly higher average dilution. The results of the simultaneous fit of the $e$ and $\mu$ trigger data using both flavor tagging methods are listed in Table VI. We find $\Delta m_d = (0.500\pm0.052)\hbar$ ps$^{-1}$, where the uncertainty is statistical only. This is consistent with the world average value $[(0.464\pm0.018)\hbar$ ps$^{-1}]$ [7]. Using the SLT tag in doubly flavor tagged events removes events with higher-than-average dilution from the JCT. This results in lower values of $N_D$ for the jet-charge flavor tag than found in the fits of the individual samples listed in Table V.

Figure 11 shows the fraction of same-sign events as a function of the reconstructed proper decay length $ct$. The points with error bars are the data. The curve is a representation of the results of the fit for $\Delta m_d$ and $N_D$. Figure 11 has been included to illustrate the clear evidence of $B^0$ mixing in the data. However, it does not contain all of the information that goes into the unbinned likelihood fit. In Fig. 11, all

TABLE VI. Results of the maximum likelihood fit for $\Delta m_d$ and the flavor tag dilution normalization parameters ($N_D$) for the $e$ and $\mu$ trigger data using both soft-lepton and jet-charge flavor tagging. The first error is the statistical error in the parameter, determined by the fit, and the second error is the systematic error, which is determined using the prescription described in the text. The dilution normalization parameters ($N_D$) for the JCT are lower than those in Table V because the SLT is used for double flavor tagged events (SLT and JCT), which lowers the average dilution for the JCT. Only the statistical errors are given for the dilution normalization parameters.

| Parameter | Fit result |
|---|---|
| $\Delta m_d$ ($\hbar$ ps$^{-1}$) | $0.500\pm0.052\pm0.043$ |
| $N^e_{D,\mathrm{JCSV}}$ | $1.43\pm0.22$ |
| $N^e_{D,\mathrm{JCDV}}$ | $1.53\pm0.16$ |
| $N^e_{D,\mathrm{SLT}}$ | $1.72\pm0.10$ |
| $N^\mu_{D,\mathrm{JCSV}}$ | $1.99\pm0.32$ |
| $N^\mu_{D,\mathrm{JCDV}}$ | $2.00\pm0.22$ |
| $N^\mu_{D,\mathrm{SLT}}$ | $2.05\pm0.16$ |

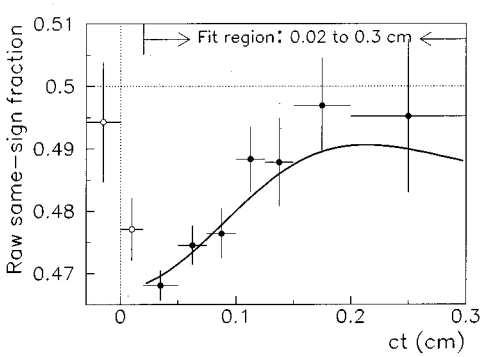


FIG. 11. The same sign fraction as a function of the proper decay length $ct$. A representation of the unbinned maximum likelihood fit for $\Delta m_d$ and the $N_D$ factors is superimposed on the data.

events are treated equally. In the fit, events are effectively weighted based on their estimated dilution.

### A. Check of fitting procedure

To check our fitting procedure, we used a fast Monte Carlo method which generated hundreds of data samples, each with the same statistics, tagging dilution, and $t$ resolution as the real data. Figure 12 shows the fit results of 400 fast Monte Carlo samples, representing the SLT flavor tagged, $e$-trigger data. The top row of plots show distributions of the fitted values of $\Delta m_d$ and $N_D$ for the 400 samples.

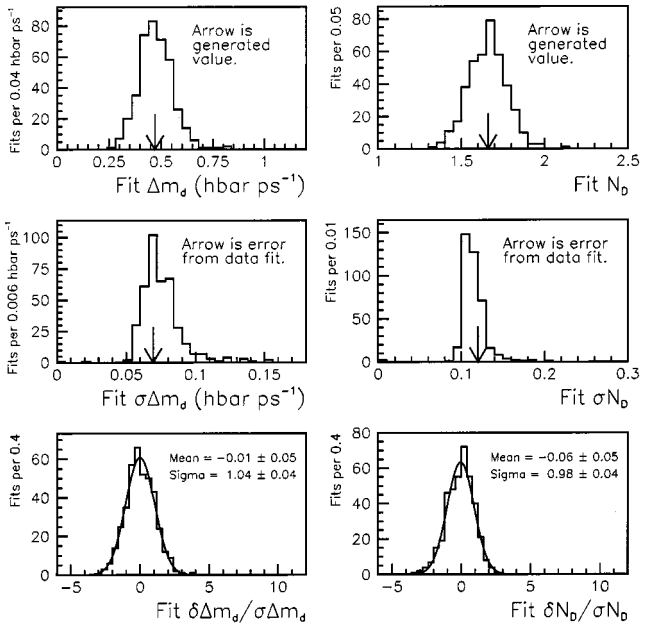


FIG. 12. Fit results for 400 fast Monte Carlo samples, simulating the $e$-trigger, SLT flavor tagged data. The top row of plots show distributions of the fitted values with arrows indicating the generated values for the samples. The middle plots show distributions of the statistical uncertainties on the fitted values with arrows indicating the statistical uncertainty for the fit to the real data. The bottom plots show distributions of the deviation from the true value, divided by the statistical uncertainty (pull distributions). The pull distributions have zero mean and unit width, as expected.

The arrows indicate the values of $\Delta m_d$ and $N_D$ with which the samples were generated. The mean of each distribution is consistent with the generation value. The middle row of plots show the distributions of the statistical uncertainty in $\Delta m_d$ and $N_D$. The arrows indicate the statistical uncertainty from the fit to the SLT flavor tagged, $e$-trigger data. The statistical uncertainties in $\Delta m_d$ and $N_D$ for the data are near the most probable values from the fast Monte Carlo samples. The bottom row of plots show the distributions of the deviation of the fitted value from the generation value divided by the statistical uncertainty for $\Delta m_d$ and $N_D$. These distributions have a mean of zero and unit width, which confirms that $\Delta m_d$ and $N_D$ are unbiased and that the statistical uncertainty is correct.

### B. Systematic uncertainties

To determine the systematic uncertainty in $\Delta m_d$, the fixed input parameters in Table IV were varied by the amounts listed in this table. To determine the systematic uncertainty associated with the dilution parametrizations, the parameters describing the $D_{\rm raw}$ dependence on $|Q_{\rm jet}|$ and $p_T^{\rm rel}$ of the soft lepton were varied by their statistical uncertainties. A systematic uncertainty to account for the possible presence of fake secondary vertices from non-heavy flavor backgrounds as well as heavy flavor events (gluon splitting) was determined using a combination of data and Monte Carlo simulations. The observed excess in the data over the combined contribution of $b\overline{b}$ and $c\overline{c}$ (see Fig. 5) was used to define the shape of this background. This shape was included in the likelihood function with a dilution that varied from 0 to $D_{b\overline{b}}$.

The systematic uncertainty assigned to the variation of each input parameter was the shift in $\Delta m_d$ from the fit result with the nominal values of the input parameters. The total systematic uncertainty is the sum in quadrature of these shifts. The same procedure was applied to the four data subsamples ($e$ SLT, $e$ JCT, $\mu$ SLT, $\mu$ JCT) to determine the systematic uncertainties for the dilution normalization factors.

The procedure described above was checked for the largest individual contributions to the systematic uncertainty using fast Monte Carlo samples. Samples generated with a variation on one of the input parameters (e.g. $\tau_{B^+}/\tau_{B^0} = 1.02 + 0.05$) were fit using the nominal parameter (e.g. $\tau_{B^+}/\tau_{B^0} = 1.02$). The average bias on the fitted values for the fast Monte Carlo samples was consistent with the deviation on the fitted values observed when the data are fit with a fixed parameter variation.

Table VII lists the individual contributions to the systematic uncertainty in $\Delta m_d$ ($\pm 0.043\hbar$ ps$^{-1}$). The largest single contribution ($\pm 0.032\hbar$ ps$^{-1}$) is the unknown soft-lepton flavor tag dilution for $c\overline{c}$ events. The SLT $c\overline{c}$ dilution was varied over the full possible range (0 to 1). If the assumed $c\overline{c}$ dilution in the fit is lower (higher) than its true value, the fraction of same-sign events at small $t$ will appear lower (higher), which biases $\Delta m_d$ low (high). The second largest contribution ($\pm 0.021\hbar$ ps$^{-1}$) is the uncertainty in the lifetime ratio of the $B^+$ and the $B^0$ mesons. If the value of

TABLE VII. The individual contributions to the systematic error in $\Delta m_d$. The value of $\delta\Delta m_d$ is the amount by which the fitted value of $\Delta m_d$ shifted when a parameter was varied. The size of the variations is given in Table IV and in the text. The parameters that were varied are the $B$ hadron lifetimes ($\tau_i$), the assumed value of $\Delta m_s$, the $B_s^0$ and $\Lambda_b$ production fractions [$f(\bar{b}\to B_s^0)$] and [$f(b\to\Lambda_b)$], the fraction of trigger leptons from sequential decay ($f_{\rm seq}$), the assumed dilution for $c\bar{c}$ events, the effective lifetime for $c\bar{c}$ events ($\tau_{c\bar{c}}$), the fraction of trigger muons that are fake and have zero dilution ($F^0_{{\rm fake}\mu}$), the normalization for the fake-vertex component, the assumed dilution for fake-vertex events ($D_{\rm FV}/D_{b\bar{b}}$), the fraction of $c\bar{c}$ events $F_{c\bar{c}}$, and the parametrization of $D_{\rm raw}$. The total systematic error is the sum of the individual contributions in quadrature.

| Parameter | $\delta\Delta m_d$ ($\hbar$ ps$^{-1}$) |
|---|---|
| $\tau_{B^0}$ | 0.004 |
| $\tau_{B^+}/\tau_{B^0}$ | 0.021 |
| $\tau_{B_s^0}$ | 0.005 |
| $\tau_{\Lambda_b}$ | 0.005 |
| $\Delta m_s$ | 0.004 |
| $f(\bar{b}\to B_s^0)$ | 0.001 |
| $f(b\to\Lambda_b)$ | 0.007 |
| $f_{\rm seq}$ | 0.004 |
| JCT $D_{c\bar{c}}/D_{b\bar{b}}$ | 0.002 |
| SLT $D_{c\bar{c}}$ | 0.032 |
| $\tau_{c\bar{c}}$ | 0.006 |
| $F^0_{{\rm fake}\,\mu}$ | 0.001 |
| Fake-vertex component | 0.006 |
| $D_{\rm FV}/D_{b\bar{b}}$ | 0.003 |
| $F_{c\bar{c}}$, $e$-trigger | 0.006 |
| $F_{c\bar{c}}$, $\mu$-trigger | 0.003 |
| JCT $D_{\rm raw}$ parametrization | 0.003 |
| SLT $D_{\rm raw}$ parametrization | 0.009 |
| Total systematic error | 0.043 |

$\tau_{B^+}/\tau_{B^0}$ in the fit is higher (lower) than its true value, the fraction of same-sign events at short $t$ values will appear larger (smaller), which biases $\Delta m_d$ high (low). The third largest contribution ($\pm 0.009\hbar$ ps$^{-1}$) is the uncertainty on the SLT raw dilution parametrization $D_{\rm raw}$ as a function of soft lepton $p_T^{\rm rel}$. The size of the variation for the SLT is shown by the dashed curves in Fig. 7. The raw dilution for events with no $p_T^{\rm rel}$ measurement was independently varied by the statistical uncertainty on the raw dilution for no-$p_T^{\rm rel}$ events.

Tables VIII and IX list the contributions to the systematic uncertainty in the dilution normalization factors for the $e$ and $\mu$ trigger data respectively. As for the systematic uncertainty in $\Delta m_d$, the largest contribution comes from the unknown dilution for $c\bar{c}$ events. The fraction of $B_s$ events, which we assume are half same-sign and half-opposite sign, and the fraction of events where the trigger lepton is from a sequential decay both affect the assignment of same-sign events. If these fractions are low (high), more (less) same-sign events will be attributed to mistags; thus they are strongly coupled to the dilution normalization. The uncertainty in the raw dilution parametrizations also has a large effect on the dilution normalization systematic uncertainty.

TABLE VIII. The individual contributions to the systematic error in the dilution normalization parameters for the $e$-trigger data $N^e_{D,i}$. The value of $\delta N^e_{D,i}$ is the amount by which the fitted value of $N^e_{D,i}$ shifted when a parameter was varied. The size of the variations is given in Table IV and in the text. These systematic errors are for the case where $\Delta m_d$ is allowed to float in the fit. The parameters that were varied are, the $B$ hadron lifetimes ($\tau_i$), the assumed value of $\Delta m_s$, the $B_s^0$ and $\Lambda_b$ production fractions [$f(\bar{b}\to B_s^0)$ and $f(b\to\Lambda_b)$], the fraction of trigger leptons from sequential decay ($f_{\rm seq}$), the assumed dilution for $c\bar{c}$ events, the effective lifetime for $c\bar{c}$ events ($\tau_{c\bar{c}}$), the normalization for the fake-vertex component, the assumed dilution for fake-vertex events ($D_{\rm FV}/D_{b\bar{b}}$), the fraction of $c\bar{c}$ events $F_{c\bar{c}}$, and the parametrization of $D_{\rm raw}$. The total systematic error is the sum of the individual contributions in quadrature.

| Parameter | $\delta N^e_{D,\rm JCSV}$ | $\delta N^e_{D,\rm JCDV}$ | $\delta N^e_{D,\rm SLT}$ |
|---|---|---|---|
| $\tau_{B^0}$ | 0.01 | 0.01 | 0.01 |
| $\tau_{B^+}/\tau_{B^0}$ | 0.01 | 0.01 | 0.01 |
| $\tau_{B_s^0}$ | 0.01 | 0.01 | 0.01 |
| $\tau_{\Lambda_b}$ | 0.00 | 0.00 | 0.00 |
| $\Delta m_s$ | 0.02 | 0.01 | 0.01 |
| $f(\bar{b}\to B_s^0)$ | 0.05 | 0.05 | 0.05 |
| $f(b\to\Lambda_b)$ | 0.01 | 0.01 | 0.01 |
| $f_{\rm seq}$ | 0.06 | 0.06 | 0.06 |
| Assumed $c\bar{c}$ dilution | 0.12 | 0.05 | 0.15 |
| $\tau_{c\bar{c}}$ | 0.00 | 0.00 | 0.01 |
| Fake-vertex component | 0.02 | 0.01 | 0.02 |
| $D_{\rm FV}/D_{b\bar{b}}$ | 0.06 | 0.03 | 0.04 |
| $F_{c\bar{c}}$ | 0.00 | 0.01 | 0.01 |
| $D_{\rm raw}$ parametrization | 0.10 | 0.05 | 0.06 |
| Total systematic error | 0.19 | 0.11 | 0.18 |

### C. Flavor tag $\epsilon D^2$

The measurement of the statistical power $\epsilon D^2$ of the flavor tagging methods is done in two steps. First, the raw $\epsilon D^2$ is calculated using the raw dilution rather than the true dilution. Then, the raw $\epsilon D^2$ is rescaled by $N_D^2$, which translates the raw dilution to the true dilution. The $N_D$ factor for each flavor tagging method in the $e$ and $\mu$ samples is determined in the unbinned maximum likelihood fit with $\Delta m_d$ fixed to the world average [22] ($0.474\hbar$ ps$^{-1}$). These $N_D$ values are given in Table V, where the first uncertainty is statistical and the second systematic.

The raw or uncorrected value of $\epsilon D^2$ is obtained by summing the $\epsilon D^2_{\rm raw}$ values in the bins of either $p_T^{\rm rel}$ for the SLT or $|Q_{\rm jet}|$ for the JCT. The efficiency for each bin is defined as

TABLE IX. The individual contributions to the systematic error in the dilution normalization parameters for the $\mu$-trigger data $N^{\mu}_{D,i}$. The value of $\delta N^{\mu}_{D,i}$ is the amount by which the fitted value of $N^{\mu}_{D,i}$ shifted when a parameter was varied. The size of the variations is given in Table IV and in the text. These systematic errors are for the case where $\Delta m_d$ is allowed to float in the fit. The parameters that were varied are the $B$ hadron lifetimes ($\tau_i$), the assumed value of $\Delta m_s$, the $B^0_s$ and $\Lambda_b$ production fractions [$f(\overline{b}\to B^0_s)$ and $f(b\to\Lambda_b)$], the fraction of trigger leptons from sequential decay ($f_{\rm seq}$), the assumed dilution for $c\overline{c}$ events, the effective lifetime for $c\overline{c}$ events ($\tau_{c\overline{c}}$), the fraction of trigger muons that are fake and have a dilution of zero ($F^0_{{\rm fake}\,\mu}$), the normalization for the fake-vertex component, the assumed dilution for fake-vertex events ($D_{\rm FV}/D_{b\overline{b}}$), the fraction of $c\overline{c}$ events $F_{c\overline{c}}$, and the parametrization of $D_{\rm raw}$. The total systematic error is the sum of the individual contributions in quadrature.

| Parameter | $\delta N^{\mu}_{D,\rm JCSV}$ | $\delta N^{\mu}_{D,\rm JCDV}$ | $\delta N^{\mu}_{D,\rm SLT}$ |
|---|---|---|---|
| $\tau_{B^0}$ | 0.00 | 0.00 | 0.01 |
| $\tau_{B^+}/\tau_{B^0}$ | 0.02 | 0.02 | 0.00 |
| $\tau_{B^0_s}$ | 0.01 | 0.01 | 0.01 |
| $\tau_{\Lambda_b}$ | 0.02 | 0.02 | 0.01 |
| $\Delta m_s$ | 0.02 | 0.01 | 0.01 |
| $f(\overline{b}\to B^0_s)$ | 0.08 | 0.07 | 0.06 |
| $f(b\to\Lambda_b)$ | 0.02 | 0.01 | 0.01 |
| $f_{\rm seq}$ | 0.15 | 0.14 | 0.13 |
| Assumed $c\overline{c}$ dilution | 0.28 | 0.03 | 0.26 |
| $\tau_{c\overline{c}}$ | 0.01 | 0.00 | 0.01 |
| $F^0_{{\rm fake}\,\mu}$ | 0.19 | 0.17 | 0.15 |
| Fake vertex component | 0.00 | 0.01 | 0.01 |
| $D_{\rm FV}/D_{b\overline{b}}$ | 0.13 | 0.08 | 0.06 |
| $F_{c\overline{c}}$ | 0.00 | 0.01 | 0.02 |
| $D_{\rm raw}$ parametrization | 0.17 | 0.03 | 0.07 |
| Total systematic error | 0.43 | 0.25 | 0.37 |

the number of events in the bin divided by the total number of events before flavor tagging. Table X lists the total efficiency, raw $\epsilon D^2$, dilution normalization, and true $\epsilon D^2$ for each of the flavor tagging methods. Taking the average of the $e$ and $\mu$ trigger data, we find $\epsilon D^2$ to be $(0.78\pm0.12\pm0.08)\%$ for the JCT and $(0.91\pm0.10\pm0.11)\%$ for the SLT where the first uncertainty is statistical and the second systematic. These $\epsilon D^2$ values are about one order of magnitude lower than typical flavor tagging techniques employed on the $Z^0$ resonance [10]; however, the large $b\overline{b}$ cross section in $p\overline{p}$ collisions at $\sqrt{s}=1.8$ TeV yields $b\overline{b}$ samples that are about one order of magnitude larger at CDF than those collected on the $Z^0$ resonance. The statistical uncertainty for our measurement of $\Delta m_d$ is still competitive with similar measurements on the $Z^0$ resonance, since our smaller $\epsilon D^2$ is compensated by our larger sample size.

The values of $\epsilon D^2$ for these flavor tags depend on the data sample in which they are used. In particular, during next run of the Tevatron, we will collect large samples of $B^0/\overline{B^0}\to J/\psi K^0_S$ [for the precise measurement of the $CP$ asymmetry parameter $\sin(2\beta)$] and hadronic $B^0_s$ decays (for the precise determination of $\Delta m_s$). The triggers used to collect these data samples will be different from the inclusive lepton trigger used to collect the data for this analysis. As a result, the $B$ hadron production properties (e.g., $p_T$ of the $B$) are different, and this affects $\epsilon D^2$. Despite these differences, the results in this paper demonstrate that both the jet-charge and the soft-lepton flavor tagging methods are viable in the environment of $p\overline{p}$ collisions.

## VII. SUMMARY

We have measured $\Delta m_d$ using soft-lepton and jet-charge flavor tagging methods. This is the first application of jet-charge flavor tagging in a hadron-collider environment. The flavor at decay was inferred from the charge of the trigger lepton, which was assumed to be the product of semileptonic $B$ decay. The initial flavor was inferred from the other $B$ in the event, either using the charge of a soft lepton or the jet charge of the other $B$. The proper time at decay for each event was determined from a partial reconstruction of the decay vertex of the $B$ that produced the trigger lepton and an

TABLE X. The statistical power $\epsilon D^2$ for the flavor tagging methods used: jet-charge single vertex (JCSV), jet-charge double vertex (JCDV), and soft-lepton tag (SLT). Results for the $e$ and $\mu$ trigger data are shown in separate rows. The sum is over bins of $p_T^{\rm rel}$ for the soft-lepton data and $|Q_{\rm jet}|$ for the jet-charge data, as shown in Figs. 7 and 9, respectively. The square of the dilution normalization factor $N_D$ is used to rescale the $\Sigma_i\epsilon_i D^2_{{\rm raw}\,i}$ value to give $\Sigma_i\epsilon_i D^2_i$. The first error is statistical, the second systematic.

| Sample | Total $\epsilon$ | $\Sigma_i\epsilon_i D^2_{{\rm raw}\,i}$ | $N_D$ | $\Sigma_i\epsilon_i D^2_i$ |
|---|---|---|---|---|
| JCSV ($e$) | $(41.55\pm0.14)\%$ | $(0.077\pm0.016)\%$ | $1.88\pm0.20\pm0.15$ | $(0.27\pm0.06\pm0.04)\%$ |
| JCDV ($e$) | $(7.44\pm0.08)\%$ | $(0.159\pm0.023)\%$ | $1.76\pm0.13\pm0.09$ | $(0.49\pm0.10\pm0.05)\%$ |
| SLT ($e$) | $(4.38\pm0.06)\%$ | $(0.329\pm0.033)\%$ | $1.72\pm0.08\pm0.11$ | $(0.97\pm0.13\pm0.12)\%$ |
| JCSV ($\mu$) | $(43.81\pm0.14)\%$ | $(0.048\pm0.012)\%$ | $2.41\pm0.29\pm0.39$ | $(0.28\pm0.06\pm0.05)\%$ |
| JCDV ($\mu$) | $(7.66\pm0.07)\%$ | $(0.113\pm0.018)\%$ | $2.14\pm0.33\pm0.25$ | $(0.52\pm0.18\pm0.12)\%$ |
| SLT ($\mu$) | $(4.54\pm0.06)\%$ | $(0.210\pm0.026)\%$ | $2.01\pm0.13\pm0.22$ | $(0.85\pm0.15\pm0.19)\%$ |

estimate of the $B$ momentum. The value of $\Delta m_d$ was determined with an unbinned maximum likelihood fit of the same-sign and opposite-sign proper-time distributions (comparing the sign of the trigger-lepton charge and the flavor tag). The statistical power of the flavor tagging methods was measured in the unbinned maximum likelihood fit by fitting for a scale factor $N_D$, for each of the flavor tagging methods, which is the ratio of the raw dilution and the true dilution.

We find $\Delta m_d = (0.500 \pm 0.052 \pm 0.043)\hbar$ ps$^{-1}$, where the first uncertainty is statistical and the second systematic. This is consistent with the world average value of $(0.464 \pm 0.018)\hbar$ ps$^{-1}$ [7] and competitive in precision with other individual measurements of $\Delta m_d$. We quantify the statistical power of the flavor tagging methods with $\epsilon D^2$, which is the tagging efficiency multiplied by the square of the dilution. We find $\epsilon D^2$ to be $(0.78 \pm 0.12 \pm 0.08)\%$ for the jet-charge flavor tag and $(0.91 \pm 0.10 \pm 0.11)\%$ for the soft-lepton flavor tag, where the first uncertainty is statistical and the second systematic. These $\epsilon D^2$ are much lower than what has been achieved in experiments on the $Z^0$ resonance; however, we have demonstrated that the much higher $b\bar{b}$ cross section at the Tevatron ($p\bar{p}, \sqrt{s} = 1.8$ TeV) can be used to compensate for the disadvantage in $\epsilon D^2$. The jet-charge and soft-lepton flavor tagging techniques will be important tools in the study of $CP$ violation in the upcoming run of the Tevatron.

## ACKNOWLEDGMENTS

We thank the Fermilab staff and the technical staffs of the participating institutions for their vital contributions. This work was supported by the U.S. Department of Energy and National Science Foundation, the Italian Istituto Nazionale di Fisica Nucleare, the Ministry of Education, Science and Culture of Japan, the Natural Sciences and Engineering Research Council of Canada, the National Science Council of the Republic of China, the Swiss National Science Foundation, and the A. P. Sloan Foundation.

## APPENDIX A: THE DILUTION NORMALIZATION FACTOR

The true dilution $D$ of a flavor tagging method is defined as

$$D = 2P_{\text{tag}} - 1, \tag{A1}$$

where $P_{\text{tag}}$ is the probability that the flavor tag is correct. An equivalent expression for $D$ is

$$D = \frac{N_T - N_M}{N_T + N_M}, \tag{A2}$$

where $N_T (N_M)$ is the number of correct (incorrect) tags in a sample of $N_{\text{total}} = N_T + N_M$ events. The raw dilution is defined as

$$D_{\text{raw}} = \frac{N_{\text{OS}} - N_{\text{SS}}}{N_{\text{OS}} + N_{\text{SS}}}, \tag{A3}$$

where $N_{\text{OS}}$ ($N_{\text{SS}}$) is the number of opposite-sign (same-sign) events in the sample, comparing the trigger-lepton charge with either the sign of the soft-lepton charge or the jet charge. If the data were pure $b\bar{b}$ with no $B$ mixing and all of the trigger leptons were from direct $B$ decay, all opposite (same) sign events would be correctly (incorrectly) flavor tagged. That is, we would have $N_T = N_{\text{OS}}$, $N_M = N_{\text{SS}}$, and $D = D_{\text{raw}}$. There are, however, several things in the data that break the $N_T = N_{\text{OS}}$ and $N_M = N_{\text{SS}}$ assumptions. They are

$B$ **mixing**: If the trigger lepton is from a $B$ hadron that decays in a state opposite its original flavor, the trigger-lepton charge will have the ''wrong'' sign. In this case, events with the correct flavor tag are same-sign.

**Sequential decays**: The charge of trigger leptons from sequential $B$ decay ($b \to c \to l\, s\, X$) is opposite that of direct $B$ decay. For trigger leptons that are from sequential decay, events with the correct flavor tag are same-sign, if the trigger-lepton $B$ did not mix.

$c\bar{c}$ **events**: Events from $c\bar{c}$ production may have a non-zero dilution that is not the same as the dilution from $b\bar{b}$ events.

**Fake leptons**: The $e$-trigger data has essentially no fake trigger electrons. However, about 12% of the $\mu$-trigger data have a hadron that faked a muon, whose charge is random (see Appendix B).

If there were no fake leptons, the number of opposite-sign and same-sign events from $b\bar{b}$ production are given by

$$N_{\text{OS}}^{b\bar{b}} = (1 - f_{\text{seq}}^{\text{ws}})[(1 - \bar{\chi}')N_T^{b\bar{b}} + \bar{\chi}' N_M^{b\bar{b}}] + f_{\text{seq}}^{\text{ws}}[\bar{\chi}' N_T^{b\bar{b}} + (1 - \bar{\chi}')N_M^{b\bar{b}}] \tag{A4}$$

$$N_{\text{SS}}^{b\bar{b}} = (1 - f_{\text{seq}}^{\text{ws}})[\bar{\chi}' N_T^{b\bar{b}} + (1 - \bar{\chi}')N_M^{b\bar{b}}] + f_{\text{seq}}^{\text{ws}}(1 - \bar{\chi}')N_T^{b\bar{b}} + \bar{\chi}' N_M^{b\bar{b}}] \tag{A5}$$

where $f_{\text{seq}}^{\text{ws}}$ is the fraction of trigger leptons in $b\bar{b}$ events that are from sequential decay in which the trigger-lepton charge has the ''wrong'' sign, $\bar{\chi}'$ is the effective[1] probability that the $B$ hadron that produced the trigger lepton decayed in a mixed state, and $N_{\text{OS}}^{b\bar{b}}$ ($N_{\text{SS}}^{b\bar{b}}$) is the number of same-sign (opposite-sign) $b\bar{b}$ events. For events from $c\bar{c}$ production we have

$$N_{\text{OS}}^{c\bar{c}} = N_T^{c\bar{c}} \tag{A6}$$

$$N_{\text{SS}}^{c\bar{c}} = N_M^{c\bar{c}} \tag{A7}$$

[1]It is an ''effective'' probability because our secondary vertexing method is inefficient for low values of $t$, which causes $\bar{\chi}'$ to be larger than $\bar{\chi}$ [7].

where $N_{\rm OS}^{c\bar{c}}$ ($N_{\rm SS}^{c\bar{c}}$) is the number of same-sign (opposite-sign) $c\bar{c}$ events. Using Eqs. (A3), (A4), (A5), (A6), and (A7) the raw dilution can be written as

$$D_{\rm raw}=\frac{(1-2\bar{\chi}')(1-2f_{\rm seq}^{\rm ws})(N_T^{b\bar{b}}-N_M^{b\bar{b}})+(N_T^{c\bar{c}}-N_M^{c\bar{c}})}{N_T^{b\bar{b}}+N_M^{b\bar{b}}+N_T^{c\bar{c}}+N_M^{c\bar{c}}}. \tag{A8}$$

If a fraction of the events ($F_{{\rm fake}\,l}^{0}$) have a fake trigger lepton whose charge-sign is random, these events will have a raw dilution of zero since the number of same-sign fake-lepton events will equal the number of opposite-sign fake-lepton events. Taking fake leptons into account gives

$$D_{\rm raw}=(1-F_{{\rm fake}\,l}^{0})\times\frac{(1-2\bar{\chi}')(1-2f_{\rm seq}^{\rm ws})(N_T^{b\bar{b}}-N_M^{b\bar{b}})+(N_T^{c\bar{c}}-N_M^{c\bar{c}})}{N_T^{b\bar{b}}+N_M^{b\bar{b}}+N_T^{c\bar{c}}+N_M^{c\bar{c}}}. \tag{A9}$$

Using Eq. (A2), we define the true flavor tagging dilution in $b\bar{b}$ and $c\bar{c}$ events as

$$D_{b\bar{b}}\equiv\frac{N_T^{b\bar{b}}-N_M^{b\bar{b}}}{N_T^{b\bar{b}}+N_M^{b\bar{b}}} \tag{A10}$$

and

$$D_{c\bar{c}}\equiv\frac{N_T^{c\bar{c}}-N_M^{c\bar{c}}}{N_T^{c\bar{c}}+N_M^{c\bar{c}}} \tag{A11}$$

respectively. The fractions of events from $b\bar{b}$ and $c\bar{c}$ production are defined by

$$F_{b\bar{b}}\equiv\frac{N_T^{b\bar{b}}+N_M^{b\bar{b}}}{N_T^{b\bar{b}}+N_M^{b\bar{b}}+N_T^{c\bar{c}}+N_M^{c\bar{c}}} \tag{A12}$$

and

$$F_{c\bar{c}}\equiv\frac{N_T^{c\bar{c}}+N_M^{c\bar{c}}}{N_T^{b\bar{b}}+N_M^{b\bar{b}}+N_T^{c\bar{c}}+N_M^{c\bar{c}}} \tag{A13}$$

respectively. Combining Eqs. (A8), (A10), (A11), (A12), (A13) gives

$$D_{\rm raw}=(1-F_{{\rm fake}\,l}^{0})[(1-2\bar{\chi}')(1-2f_{\rm seq}^{\rm ws})F_{b\bar{b}}D_{b\bar{b}}+F_{c\bar{c}}\ D_{c\bar{c}}]$$

$$D_{\rm raw}=\left\{(1-F_{{\rm fake}\,l}^{0})\left[(1-2\bar{\chi}')(1-2f_{\rm seq}^{\rm ws})F_{b\bar{b}}+F_{c\bar{c}}\frac{D_{c\bar{c}}}{D_{b\bar{b}}}\right]\right\}D_{b\bar{b}}$$

$$D_{\rm raw}=\frac{1}{N_D}D_{b\bar{b}} \tag{A14}$$

where we have defined the dilution normalization factor $N_D$ as

$$\frac{1}{N_D}\equiv(1-F_{{\rm fake}\,l}^{0})\left[(1-2\bar{\chi}')(1-2f_{\rm seq}^{\rm ws})F_{b\bar{b}}+F_{c\bar{c}}\frac{D_{c\bar{c}}}{D_{b\bar{b}}}\right]. \tag{A15}$$

Equation (A15) can be used to calculate the expected values for the $N_D$ parameters. For this calculation, we will assume

(1) $\bar{\chi}'\approx 0.20$ from the Monte Carlo samples.

(2) $f_{\rm seq}^{\rm ws}(e\ \text{trigger})=0.07$ and $f_{\rm seq}^{\rm ws}(\mu\ \text{trigger})=0.10$ using $f_{\rm seq}^{\rm ws}=0.75\times f_{\rm seq}$ and the values in Table IV.

(3) The $F_{b\bar{b}}$ values are given in Table I. We also use $F_{c\bar{c}}=1-F_{b\bar{b}}$.

(4) For the JCT, we assume $D_{c\bar{c}}/D_{b\bar{b}}({\rm JCT})=0.5$. Using the average SLT dilution and the assumption that $D_{c\bar{c}}({\rm SLT})=0.5$, we estimate $D_{c\bar{c}}/D_{b\bar{b}}({\rm SLT})\approx 1.3$.

Using the numbers above, we find

$N_{D,{\rm SLT}}^{e}\approx 1.8$.

$N_{D,{\rm SLT}}^{\mu}\approx 2.1$.

$N_{D,{\rm JCSV}}^{e}\approx N_{D,{\rm JCDV}}^{e}\approx 1.9$.

$N_{D,{\rm JCSV}}^{\mu}\approx N_{D,{\rm JCDV}}^{\mu}\approx 2.4$.

## APPENDIX B: FRACTION OF FAKE TRIGGER MUONS

As is stated in Sec. IV C, we believe that most of the fake trigger muons in the data are from heavy flavor decay. There may be some correlation on average between the sign fake muon charge and the $B$ flavor at decay, however we assume that this correlation is smaller than that of real trigger muons. Fake muon events are divided into two groups:

(1) Fake muon events whose dilution is the same as the dilution for real muons.

(2) Fake muon events whose dilution is zero.

We treat group 1 as if they are real trigger-muon events. We treat group 2 as if they are $b\bar{b}$ events with a flavor tagging dilution of zero.

We determine the fraction of events with fake muons that have zero dilution in the $\mu$-trigger data by assuming that the *true* flavor tagging dilution is the same in the $e$ and $\mu$ trigger data. The raw dilution ($D_{\rm raw}$), which assumes all opposite-sign (same-sign) events are tags (mistags), is different for the $e$ and $\mu$ trigger data for the following reasons:

(1) The fraction of real trigger leptons in $b\bar{b}$ events that are not from direct $b\to l$ decay ($f_{\rm seq}$) is 9.4% for the $e$-trigger data and 13.6% for the $\mu$-trigger data.

(2) The fraction of events from $c\bar{c}$ production $F_{c\bar{c}}$ is slightly different (see Table I).

(3) We estimate that only 1% of the trigger electrons are fake, while, as shown below, about 10% of the $\mu$-trigger events contain a fake muon.

We can correct $D_{\rm raw}$ for (1) and (2) using the equation

$$\langle D'_{\rm raw}\rangle=\frac{\langle D_{\rm raw}\rangle}{F_{b\bar{b}}\cdot(1-2f_{\rm seq}^{\rm ws}+F_{c\bar{c}}\cdot D_{c\bar{c}}/D_{b\bar{b}})} \tag{B1}$$

TABLE XI. Average raw dilution for three flavor taggers in the electron and muon data corrected for wrong sign sequential decay trigger leptons and the $b\bar{b}$ to $c\bar{c}$ ratio.

| Flavor tag | $\langle D_{\rm raw}\rangle$ | Correction | $\langle D'_{\rm raw}\rangle$ | $\langle D'_{\rm raw}(e)\rangle/\langle D'_{\rm raw}(\mu)\rangle$ |
|---|---|---|---|---|
| JCSV ($e$) | $(2.7\pm0.5)\%$ | 1.16 | $(3.1\pm0.6)\%$ | $1.07\pm0.28$ |
| JCSV ($\mu$) | $(2.3\pm0.4)\%$ | 1.26 | $(2.9\pm0.5)\%$ | |
| JCDV ($e$) | $(12.1\pm1.1)\%$ | 1.15 | $(14.2\pm1.3)\%$ | $1.18\pm0.16$ |
| JCDV ($\mu$) | $(9.7\pm1.0)\%$ | 1.24 | $(12.0\pm1.2)\%$ | |
| SLT ($e$) | $(22.1\pm1.3)\%$ | 1.15 | $(25.5\pm1.5)\%$ | $1.13\pm0.10$ |
| SLT ($\mu$) | $(18.2\pm1.3)\%$ | 1.24 | $(22.5\pm1.6)\%$ | |

where $f_{\rm seq}^{\rm ws}$ is the fraction of non $b\to l$ decays that have the ''wrong'' sign. The Monte Carlo simulation gives $f_{\rm seq}^{\rm ws}=0.75f_{\rm seq}$. The values of $\langle D'_{\rm raw}\rangle$ for the SLT, JCSV, and JCDV flavor tagging methods in the $e$- and $\mu$-trigger data are given in Table XI. The weighted average of $\langle D'_{\rm raw}(e)\rangle/\langle D'_{\rm raw}(\mu)\rangle$ for the SLT, JCSV, and JCDV flavor tagging methods gives $1.14\pm0.08$. The fraction of events with fake muons that have zero dilution can be extracted using

$$F^0_{{\rm fake}\,\mu}=1-\frac{1}{\langle D'_{\rm raw}(e)\rangle/\langle D'_{\rm raw}(\mu)\rangle}. \tag{B2}$$

Equation (B2) gives $F^0_{{\rm fake}\,\mu}=(12\pm6)\%$. The relatively large uncertainty in $F^0_{{\rm fake}\,\mu}$ gives a significant systematic uncertainty in the dilution normalization $N_D$ for the flavor tags (see Table IX); however, the contribution to the systematic uncertainty in $\Delta m_d$ is relatively small.


[1] S.L. Glashow, Nucl. Phys. **22**, 579 (1961); S. Weinberg, Phys. Rev. Lett. **19**, 1264 (1967); A. Salam, in *Elementary Particle Theory: Relativistic Groups and Analyticity (Nobel Symposium No. 8)*, edited by N. Svartholm (Almqvist and Wiksell, Stockholm, 1969), p. 367.

[2] N. Cabibbo, Phys. Rev. Lett. **10**, 531 (1963); M. Kobayashi and K. Maskawa, Prog. Theor. Phys. **49**, 652 (1973).

[3] CDF Collaboration, R. Blair *et al.*, ''The CDFII Detector Technical Design Report,'' Report No. FERMILAB-PUB-96/390-E.

[4] CDF Collaboration, F. Abe *et al.*, Phys. Rev. D **59**, 032004 (1999); **58**, 112004 (1998); CDF Collaboration, F. Abe *et al.*, *ibid.* **58**, 092002 (1998); CDF Collaboration, F. Abe *et al.*, *ibid.* **57**, 5382 (1998); CDF Collaboration, F. Abe *et al.*, *ibid.* **55**, 1142 (1997); CDF Collaboration, F. Abe *et al.*, *ibid.* **77**, 1945 (1997); CDF Collaboration, F. Abe *et al.*, *ibid.* **53**, 3496 (1996).

[5] CDF Collaboration, F. Abe *et al.*, Plus. Rev. D **60**, 051101 (1999).

[6] CDF Collaboration, F. Abe *et al.*, Phys. Rev. Lett. **80**, 2057 (1998); CDF Collaboration, F. Abe *et al.*, Phys. Rev. D **59**, 032001 (1999).

[7] The Particle Data Group, C. Caso *et al.*, Eur. Phys. J. C **3**, 1 (1998).

[8] CDF Collaboration, F. Abe *et al.*, Phys. Rev. Lett. **81**, 5513 (1998).

[9] A summary of published measurements and their average can be found in Particle Data Group [7].

[10] ALEPH Collaboration, D. Buskulic *et al.*, Z. Phys. C **75**, 397 (1997); DELPHI Collaboration, P. Abreu *et al.*, *ibid.* **72**, 17 (1996); OPAL Collaboration, R. Akers *et al.*, Phys. Lett. B **327**, 411 (1994); SLD Collaboration, K. Abe *et al.*, Phys. Rev. Lett. **74**, 2890 (1995).

[11] F. Abe *et al.*, Nucl. Instrum. Methods Phys. Res. A **271**, 387 (1988).

[12] F. Abe *et al.*, Phys. Rev. Lett. **74**, 2626 (1995); see also F. Abe *et al.*, Phys. Rev. D **50**, 2966 (1994).

[13] D. Amidei *et al.*, Nucl. Instrum. Methods Phys. Res. A **350**, 73 (1994); P. Azzi *et al.*, *ibid.* **360**, 137 (1995).

[14] G.W. Foster *et al.*, Nucl. Instrum. Methods Phys. Res. A **269**, 93 (1988).

[15] $\Delta R=\sqrt{(\Delta\phi)^2+(\Delta\eta)^2}$ where $\phi$ is the azimuthal direction with respect to the beam and $\eta$ is the pseudorapidity, which is defined as $\eta=-\ln[\tan(\theta/2)]$.

[16] H.U. Bengtsson and T. Sjöstrand, Comput. Phys. Commun. **43**, 43 (1987); T. Sjöstrand, *ibid.* **82**, 74 (1994).

[17] C. Peterson *et al.*, Phys. Rev. D **27**, 105 (1983).

[18] P. Avery, K. Read, and G. Trahern, Cornell Internal Note No. CSN-22, 1985.

[19] This efficiency parametrization followed the functional form: $A$ Freq$[(p_T-B_1)/C_1]$Freq$[(p_T-B_2)/C_2]$, where $A=0.927$, $B_1=6.18$ GeV/$c$, $C_1=4.20$ GeV/$c$, $B_2=7.48$ GeV/$c$, and $C_2=0.504$ GeV/$c$. The efficiency curve turns on at $p_T=6$ GeV/$c$, rises to 50% at $p_T=8$ GeV/$c$, and has a plateau value of 93%.

[20] F. Paige and S.D. Protopopescu, Brookhaven National Laboratory Report No. BNL 38034, 1986.

[21] F. James, CERN Program library long writeup D506.

[22] The Particle Data Group, R.M. Barnett *et al.*, Phys. Rev. D **54**, 1 (1996).